iScience

CellPress
OPEN ACCESS

Article

Chimpanzee adenovirus-mediated multiple gene therapy for age-related macular degeneration

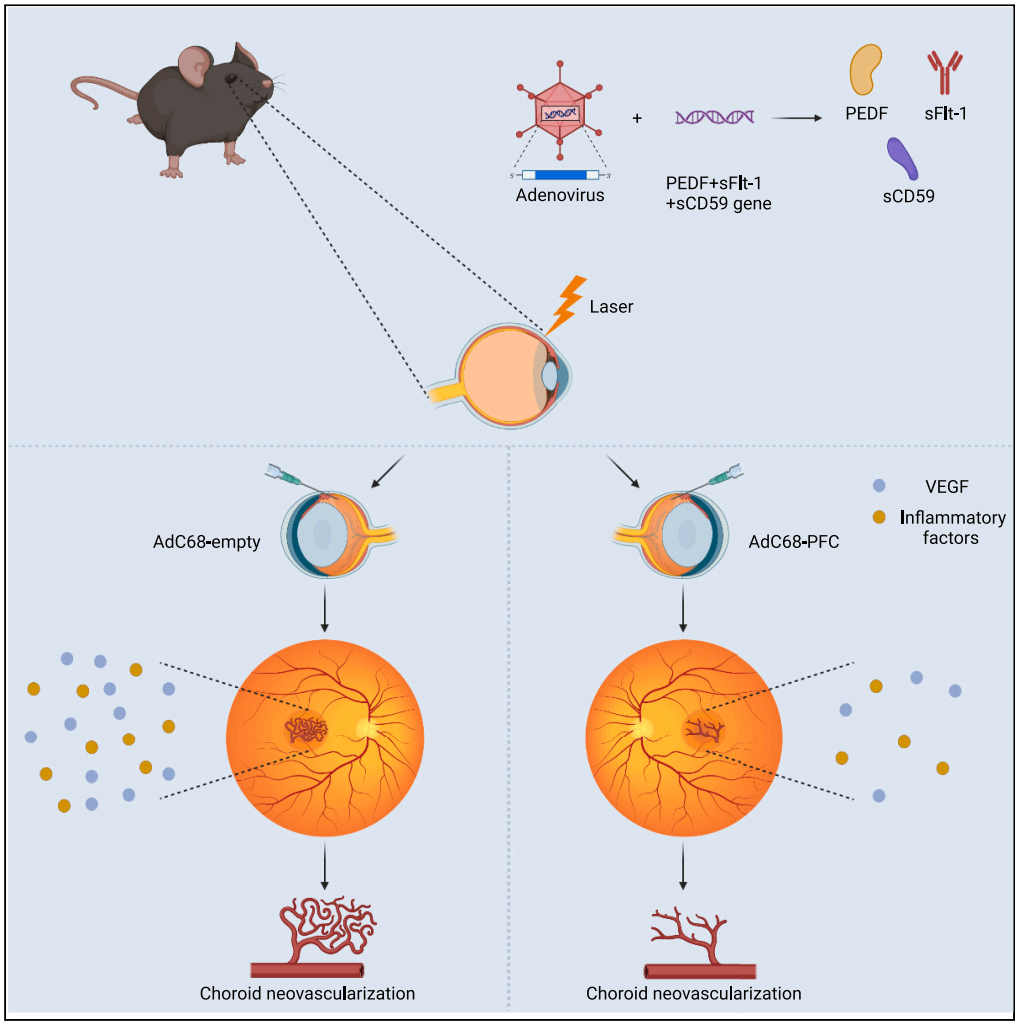

Selena Wei-Zhang, Bohao Cui, Man Xing, ..., Xiaohong Wang, Dongming Zhou, Hua Yan

xiaohongwang@tmu.edu.cn (X.W.)
zhoudongming@tmu.edu.cn (D.Z.)
zyyyanhua@tmu.edu.cn (H.Y.)

Highlights

AdC68-PFC can effectively mediate the gene expression of secreted proteins

AdC68-PFC showed a strong therapeutic effect on vascular and inflammatory phenotypes

AdC68-PFC was superior to conbercept, especially in the long-term follow-up

The safety test suggested no evidence of *in vivo* toxicity of AdCs in mouse eyes

Wei-Zhang et al., iScience *26*, 107939
October 20, 2023
https://doi.org/10.1016/j.isci.2023.107939

iScience

CellPress
OPEN ACCESS

Article

Chimpanzee adenovirus-mediated multiple gene therapy for age-related macular degeneration

Selena Wei-Zhang,[1,2,3,6] Bohao Cui,[1,2,6] Man Xing,[3] Jiaojiao Liu,[3] Yingying Guo,[3] Kai He,[1,2] Tinghui Bai,[1,2,3] Xue Dong,[1,2] Yi Lei,[1,2] Wei Zhou,[1] Hui Zhou,[1] Shengnan Liu,[1] Xiaohong Wang,[1,2,4,*] Dongming Zhou,[3,*] and Hua Yan[1,2,5,7,*]

SUMMARY

Neovascular age-related macular degeneration AMD (nAMD) is characterized by choroidal neovascularization (CNV) and could lead to irreversible blindness. However, anti-vascular endothelial growth factor (VEGF) therapy has limited efficacy. Therefore, we generated a chimpanzee adenoviral vector (AdC68-PFC) containing three genes, pigment endothelial-derived factor (PEDF), soluble fms-like tyrosine kinase-1 (sFlt-1), and soluble forms of CD59 (sCD59), to treat nAMD. The results showed that AdC68-PFC mediated a strong onset of PEDF, sFlt-1, and sCD59 expression both *in vivo* and *in vitro*. AdC68-PFC showed preventive and therapeutic effects following intravitreal (IVT) injection in the laser-induced CNV model and very low-density lipoprotein receptor-deficient (*Vldlr*$^{-/-}$) mouse model. *In vitro* assessment indicated that AdC68-PFC had a strong inhibitory effect on endothelial cells. Importantly, the safety test showed no evidence of *in vivo* toxicity of adenovirus in murine eyes. Our findings suggest that AdC68-PFC may be a long-acting and safe gene therapy vector for future nAMD treatments.

INTRODUCTION

Age-related macular degeneration (AMD) is currently the leading cause of vision loss in the elderly population over 60 years of age.[1] Neovascular AMD (nAMD) is a late stage of AMD, which is characterized by choroidal neovascularization (CNV), leading to several typical lesions, including retinal hemorrhage, retinal pigment epithelial detachments, or hard exudate.[2] Although nAMD only accounts for approximately 20% of patients with AMD, it is responsible for approximately 90% of the severe central vision loss caused by AMD.[3] Anti-vascular endothelial growth factor (VEGF) therapy is currently the first-line treatment for nAMD, but repetitive intraocular injections of anti-VEGF drugs may lead to several risks, including increased intraocular pressure and severe endophthalmitis.[4,5] According to previous studies, vision gains during the first 2 years were not retained after 5 or 7 years in two-thirds of patients who received anti-VEGF monotherapy.[6,7] Considering that nAMD is a complicated and multifactorial disease, we attempted to develop a multitargeted approach that simultaneously targets VEGF and other essential factors.

The exact mechanism of AMD pathogenesis remains unknown, but the damage in the retinal pigment epithelium (RPE), associated immune responses, and degenerative changes within the choroidal vasculature are believed to drive the production of VEGFA, which is found vital in nAMD. Examination of early AMD lesions indicated that loss of vessels and/or reduction of perfusion in the choroidal vasculature is often accompanied by the accumulation of macrophages.[8] Meanwhile, complement components, including C3a, C5, and the sublytic membrane attack complex (MAC), reportedly induce VEGF expression and promote CNV.[9] Currently, many studies have focused on the development of combined therapies that target angiogenesis or other involved pathways, which are superior to anti-VEGF monotherapy. Remarkably, preclinical assessment and clinical trials have proven the safety profile and efficacy of multitarget drugs, including ABBV642, faricimab, and efdamrofusp alfa.[9–11]

Gene therapy offers sustained delivery of foreign genes and has been widely used in retinal diseases. The retina has unique advantages as a target organ in gene therapy. The intraocular environment and blood-retinal barrier provide the retina with a degree of immune privilege, which suppresses immune responses that could adversely affect the retinal function expression of the therapeutic gene.[12] Recombinant adeno-associated virus (AAV)-based vectors are well-accepted gene delivery vehicles for gene transfer to retinal cells because of their sustained levels of gene expression, low toxicity, and immunogenicity. Although most clinical applications currently employ AAV vectors, the small

[1]Department of Ophthalmology, Tianjin Key Laboratory of Ocular Trauma, Tianjin Medical University General Hospital, Tianjin Medical University, Tianjin, China
[2]Laboratory of Molecular Ophthalmology, Tianjin Medical University, Tianjin 300070, China
[3]Department of Pathogen Biology, School of Basic Medical Sciences, Tianjin Medical University, Tianjin, China
[4]Department of Pharmacology, Tianjin Key Laboratory of Inflammation Biology, School of Basic Medical Sciences, Tianjin Medical University, Tianjin, China
[5]School of Medicine, Nankai University, Tianjin, China
[6]These authors contributed equally
[7]Lead contact
*Correspondence: xiaohongwang@tmu.edu.cn (X.W.), zhoudongming@tmu.edu.cn (D.Z.), zyyyanhua@tmu.edu.cn (H.Y.)
https://doi.org/10.1016/j.isci.2023.107939

packaging capability (4.7 kb) is a limitation for them.[13] In this study, chimpanzee adenoviral vectors (AdCs) were used owing to their large capacity, relatively lower level of seroprevalence, and neutralizing antibodies compared with human adenovirus type C5-based vectors.[14]

To further utilize the concept of a multitargeted approach, we developed a multigenic AdC with both anti-angiogenic and anti-inflammatory effects, enabling the simultaneous expression of three different genes: pigment endothelial-derived factor (PEDF), soluble fms-like tyrosine kinase-1 (sFlt-1), and soluble forms of CD59 (sCD59). All three genes have been used in clinical trials of gene therapy for AMD, and their clinical efficacy and safety in patients with AMD have been proven (ClinicalTrials.gov: NCT00109499, NCT01494805, NCT01024998, NCT03585556, NCT03144999). To connect the two different genes, a 2A peptide derived from porcine teschovirus-1 (P2A) was used because it exhibited a high cleavage efficiency.[15] Our data suggest that the dual-acting AdC is a potential therapeutic tool for future gene therapy in AMD and other neovascular eye diseases.

RESULTS

Development and validation of multigenic AdCs *in vitro*

We generated multigenic AdC68 gene therapy vectors by inserting an additional expression cassette into the E1 deleted region of the AdC68 genome. The expression cassette included a codon-optimized sequence of PEDF, sFlt-1, and sCD59, and the cleavable linker P2A was used to connect two different genes, resulting in the generation of AdC68-PEDF-P2A-sFlt-1-P2A-sCD59 (AdC68-PFC) (Figure S1A). AdC68-eGFP (Figure S2A) was used to visualize the expression of the AdCs. Western blot analysis confirmed the dose-dependent expression of PEDF, sFlt-1, and sCD59 in the cell lysate and supernatant of ARPE-19 cells (Figure S1B) and human umbilical vascular endothelial cells (HUVECs) (Figure S2B), respectively. Accordingly, dose-dependent and time-dependent expression of eGFP signal was detected in ARPE-19 cells (Figure S1C) and HUVECs (Figure S2C), respectively.

AdCs injection efficiently delivers foreign genes into the retina/choroid

To examine the kinetics of transgene expression mediated by AdCs via intravitreal (IVT) injection, AdC68-eGFP was administered at two different doses (1.5×10^9 viral particles (vp) and 7.5×10^9 vp) per eye. The eGFP signal mediated by AdCs was readily detected as early as 48 h post-injection by *ex vivo* fluorescence microscopy and could last approximately 35 days (Figure 1A). We next injected AdC68-PFC into wild-type mouse eyes at two different doses (1.5×10^9 vp and 7.5×10^9 vp) per eye and evaluated the PEDF, sFlt-1, and sCD59 mRNA copy number 4 days after injection by qPCR analysis. Robust expression of PEDF, sFlt-1, and sCD59 mRNA was detected in the two AdC68-PFC groups, and the low-dose (1.5×10^9 vp) AdC68-PFC group expressed a relatively lower level of the three mRNAs, compared with the high-dose (7.5×10^9 vp) AdC68-PFC group (Figures 1B–1D). To test the expression of PEDF, sFlt-1, and sCD59 at the protein level, western blot analyses were performed 7 days after treatment with 7.5×10^9 vp AdC68-PFC. The results clearly showed robust expression of PEDF, sFlt-1, and sCD59 protein in the eyes of the mice (Figures 1E–1H).

Overall, the data suggest the potential for AdC68-PFC to neutralize VEGF and inflammatory factors, and consequently, to attenuate CNV. The previously described data suggested that AdC was successfully constructed and that the three target genes could be successfully expressed in a dose-dependent manner. In addition, the expression of target genes carried by AdCs via IVT injection was sustained for 2–35 days.

Administration of AdC68-PFC prevents the progression of laser-induced CNV

The previously described results indicate the successful expression of the three therapeutic genes. Thus, to further test whether AdC68-PFC could attenuate CNV, the laser-induced CNV model was employed, in which laser burn was used to rupture Bruch's membrane and induce vessel growth from the choroid.[16] The mice were treated with PBS (negative control), AdC68-empty (sham control), or AdC68-PFC at day 4. Conbercept, which was also used as the positive control, was injected at day 1. Laser burns were administered at day 0 (Figure 2A). Fundus fluorescent angiography (FFA) results revealed that compared to the other three groups, AdC68-PFC efficiently reduced the CNV leakage area at days 7 and 14 (Figures 2B–2D). However, the preventive effect of conbercept was not significant.

Since neovascularization and inflammation have been implicated in the pathological process of CNV, CD31 and F4/80 were stained on flat-mounted RPE-choroid 7 and 14 days after laser burn to test whether AdC68-PFC exerts significant anti-angiogenic and anti-inflammatory effects in the laser-induced CNV model (Figure 2E).[17,18] CD31+-positive area measurements revealed a statistically significant reduction in the size of neovascularization in mice injected with AdC68-PFC 7 and 14 days after laser, compared with animals receiving PBS, AdC68-empty, and conbercept (Figures 2F and 2G). F4/80+-positive area measurements suggested that at 7 and 14 days after laser, the size of macrophage infiltration decreased in the AdC68-PFC group compared to the PBS, AdC68-empty, and conbercept groups (Figures 2H and 2I).

Furthermore, RPE-choroid flat mounts of laser spots were stained with MAC to test whether the AdC68-PFC could inhibit complement activation (Figure S3). In our study, the results suggested that 7 days after laser, there was a significant reduction in MAC deposition in the AdC68-PFC group compared with the AdC68-empty group (Figure S3C).

Taken together, our data showed that AdC68-PFC could prevent angiogenesis, macrophage infiltration, and MAC deposition, thus inhibiting the development of vascular leakage in CNV, which was superior to conbercept.

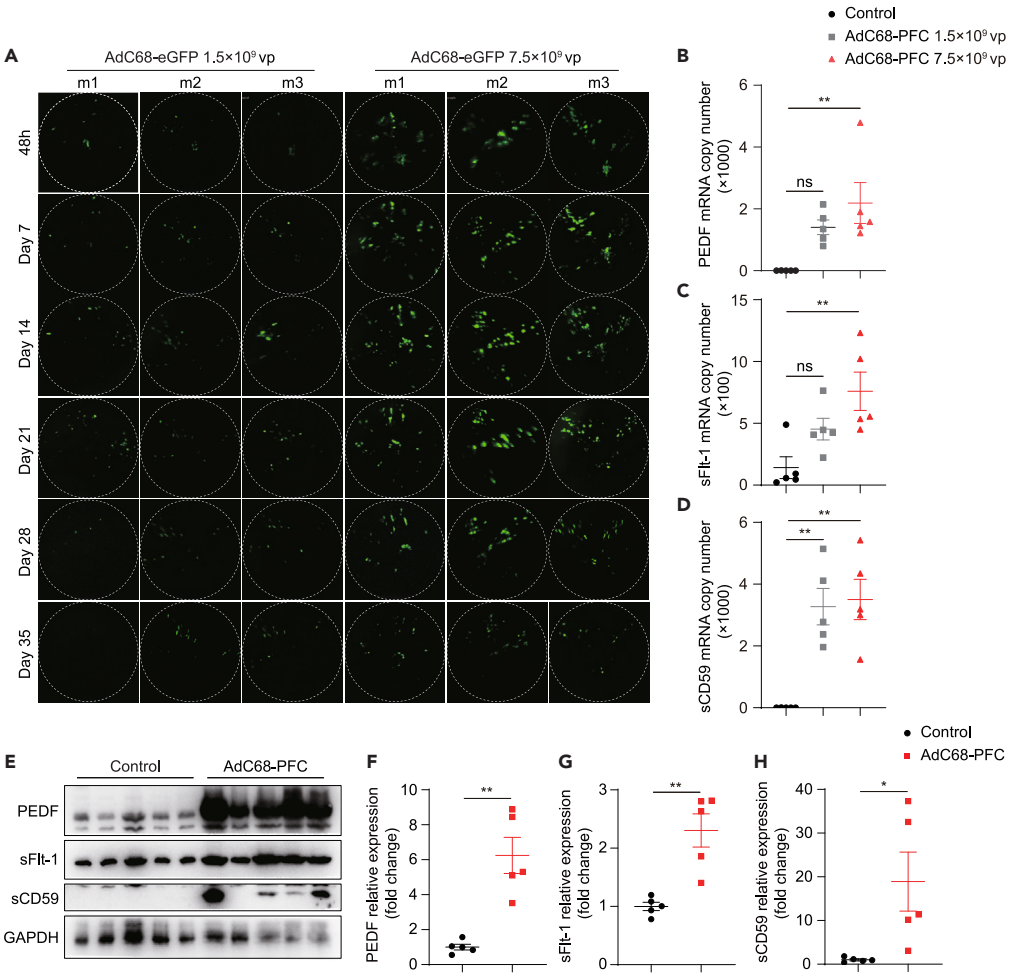

Figure 1. *In vivo* expression of eGFP, PEDF, sFlt-1, and sCD59 following IVT administration of AdCs

(A) Representative fundus images of the retina from individual mice following IVT injection of 1.5×10^9 vp and 7.5×10^9 vp AdC68-eGFP. The eGFP signal could be detected from 48 h to 35 days post-injection. The dotted circles represent the edge of mouse retina.

(B–D) Assessment of PEDF, sFlt-1, and sCD59 mRNA expression in retina-choroid-sclera complexes isolated from 10 mice. In each mouse, one eye was injected with AdC68-PFC (five mice for 1.5×10^9 vp and five mice for 7.5×10^9 vp) whereas the contralateral, un-injected eye served as control (only five eyes were used for analysis). At 4 days post-injection, RNA was purified from the retina-choroid complexes and real-time qPCR was conducted. Absolute number of mRNA copies were calculated using the standard curve method.

(E–H) Images of western blot and quantification of the PEDF, sFlt-1, and sCD59 protein amount expressed in retina-choroid complexes of five mice. In each mouse, one eye was injected with AdC68-PFC (7.5×10^9 vp) whereas the contralateral, un-injected eye served as control. Total protein was obtained from retina-choroid-sclera complexes isolated from AdC68-PFC-treated (7.5×10^9 vp) and un-injected eyes 7 days post-injection. Antibodies against GAPDH were used for the internal control. The relative expression of PEDF, sFlt-1, and sCD59 in the un-injected eyes was set to 1. Data are expressed as mean ± SEM, and analyzed using one-way ANOVA multiple comparisons with Tukey's method among groups in (B) and Student's *t* test (two-tailed) in (C) (*$p < 0.05$, **$p < 0.01$). PEDF, pigment epithelium-derived factor; sFlt-1, soluble fms-like tyrosine kinase-1; sCD59, soluble forms of CD59; IVT, intravitreal.

Treatment with AdC68-PFC therapeutically inhibits laser-induced CNV lesions

To verify whether AdC68-PFC therapeutically inhibits CNV, we designed a therapeutic strategy to better simulate the process of disease progression and treatment (Figure 3A). In brief, we applied laser-induced CNV model at day 0 and subsequently injected mice with PBS, low-dose AdC68-empty (1.5×10^9 vp), low-dose AdC68-PFC (1.5×10^9 vp), high-dose AdC68-empty (7.5×10^9 vp), high-dose AdC68-PFC (7.5×10^9 vp), or conbercept at day 1 post-laser. Notably, 1.5×10^9 vp (low dose) AdC68-PFC showed no obvious effect in this case. This might be due to acute injury-related angiogenesis and inflammation in the laser-induced CNV model, which fundamentally differs from the genetically influenced, long-standing senescent degeneration and chronic pathology of AMD.[19] Therefore, we added another high-dose (7.5×10^9 vp) AdCs group. Although the results showed a trend of low-dose AdC68-PFC in reducing the CNV leakage area, there was no statistically significant difference between the low-dose AdC68-PFC and low-dose AdC68-empty groups (Figures 3C and 3D). In contrast, compared with high-dose

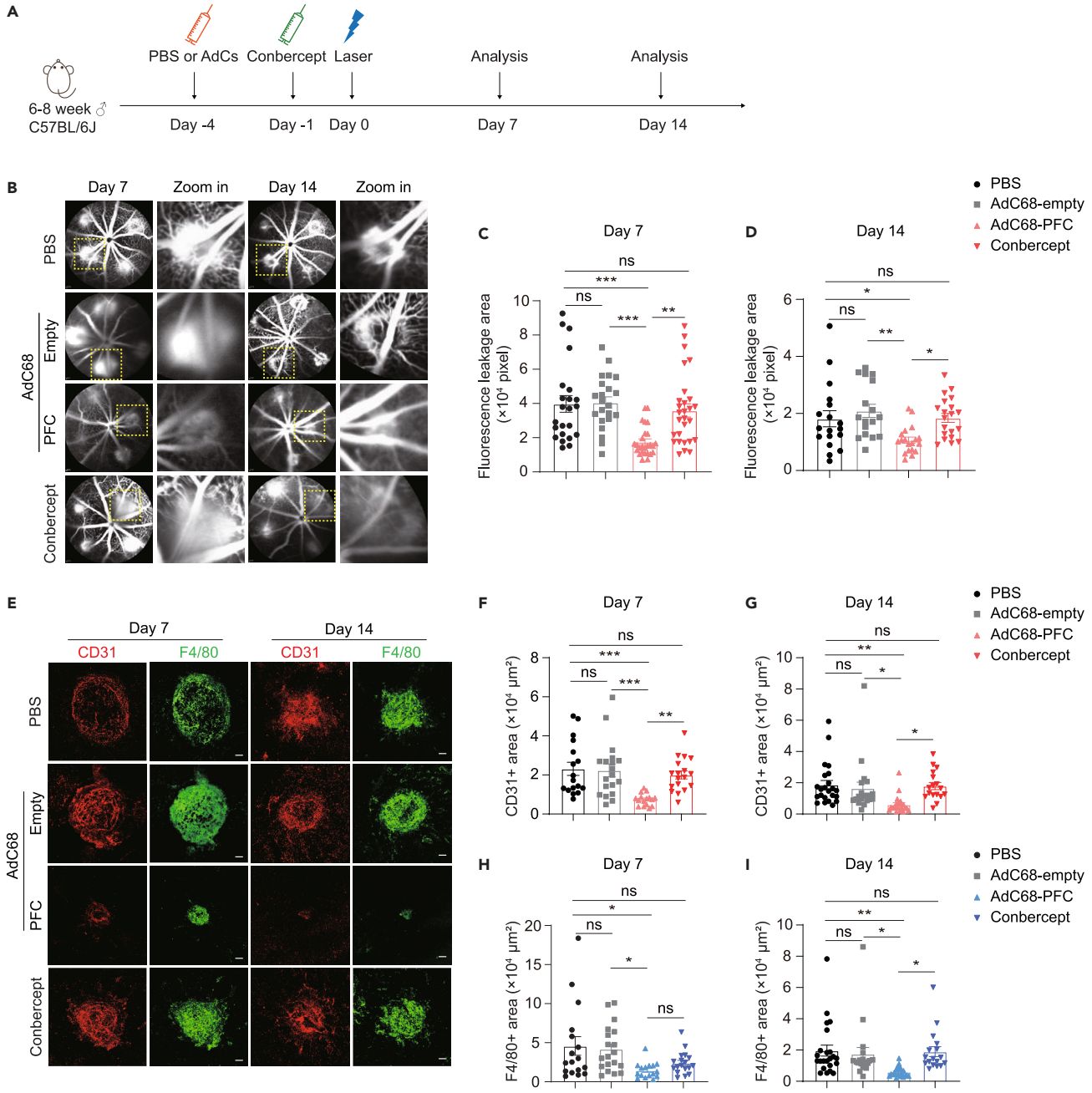

Figure 2. AdC68-PFC prevents angiogenesis and F4/80+ cells infiltration in laser-induced CNV model

(A) Schematic illustrates chronological order of IVT injections, induction of CNV and analysis. PBS and AdCs (1.5×10^9 vp) were intravitreally injected at day −4, and conbercept (10 mg/mL, 1.5 μL) was intravitreally injected at day 1. CNV was laser induced at day 0, and analysis was performed at day 7 and day 14.

(B) Representative FFA images show vascular leakage from mice undergoing indicated prophylaxis after laser-induced CNV at day 7 and 14.

(C and D) Quantification of the leakage area shown in (B) (n = 22–28 lesions from 6 to 9 eyes per group for day 7; n = 17–20 lesions from 6 to 8 eyes per group for day 14).

(E) Representative confocal images of RPE-choroid flat mounts stained with CD31 and F4/80. Scale bars, 50 μm.

(F and G) Quantification of the CNV area in (E), calculated as $CD31^+$ area at the site of laser photocoagulation at day 7 and 14. (n = 16–19 lesions from 5 to 6 eyes per group for day 7; n = 17–23 lesions from 5 to 7 eyes per group for day 14).

(H and I) Quantification of the macrophages infiltration area in (E) calculated as F4/80+ area surrounding the CNV lesion at day 7 and day 14. (n = 16–19 lesions from 5 to 6 eyes per group for day 7; n = 17–23 lesions from 5 to 7 eyes per group for day 14). Data are expressed as mean ± SEM, and analyzed using one-way ANOVA multiple comparisons with Tukey's method among groups in (C), (D), and (F–I) (*$p < 0.05$, **$p < 0.01$, ***$p < 0.001$, ****$p < 0.0001$). CNV, choroidal neovascularization; FFA, fundus fluorescent angiography.

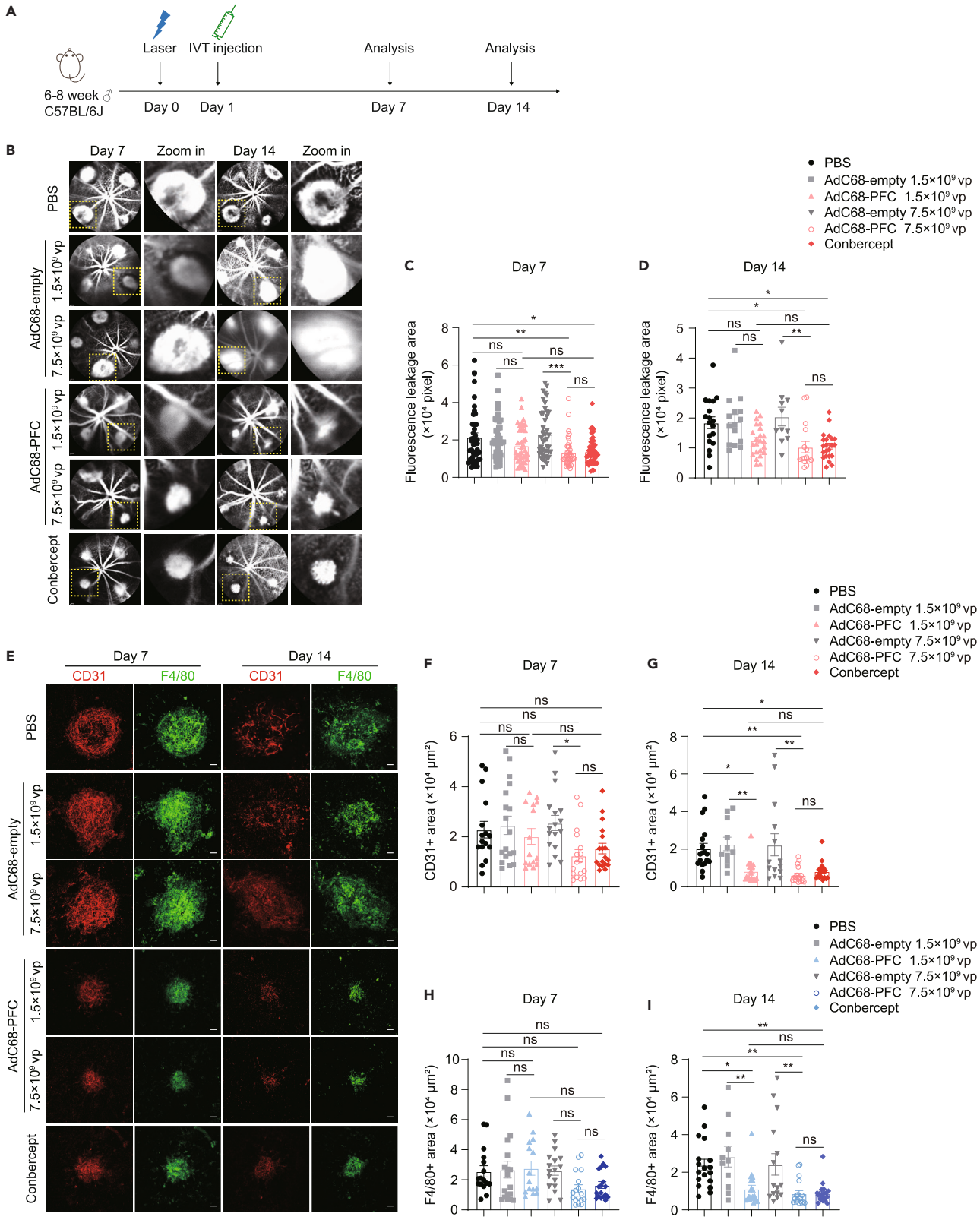
A
Laser
IVT injection
Analysis
Analysis
6-8 week ♂
C57BL/6J
Day 0
Day 1
Day 7
Day 14
B
Day 7
Zoom in
Day 14
Zoom in
PBS
AdC68-empty
1.5×10⁹ vp
7.5×10⁹ vp
AdC68-PFC
1.5×10⁹ vp
7.5×10⁹ vp
Conbercept
PBS
AdC68-empty 1.5×10⁹ vp
AdC68-PFC 1.5×10⁹ vp
AdC68-empty 7.5×10⁹ vp
AdC68-PFC 7.5×10⁹ vp
Conbercept
C
Day 7
Fluorescence leakage area (×10⁴ pixel)
D
Day 14
Fluorescence leakage area (×10⁴ pixel)
E
Day 7
Day 14
CD31
F4/80
CD31
F4/80
F
Day 7
CD31+ area (×10⁴ μm²)
G
Day 14
CD31+ area (×10⁴ μm²)
H
Day 7
F4/80+ area (×10⁴ μm²)
I
Day 14
F4/80+ area (×10⁴ μm²)
ns

Figure 3. AdC68-PFC inhibits angiogenesis and F4/80+ cells infiltration in laser-induced CNV model

(A) Schematic illustrates chronological order of IVT injections, induction of CNV, and analysis. CNV was laser induced at day 0, and PBS, AdCs (1.5×10^9 vp and 7.5×10^9 vp), and conbercept (10 mg/mL, 1.5 μL) were injected at day 1. Analysis was performed at day 7 and 14.

(B) Representative FFA images show vascular leakage from mice undergoing indicated treatment after laser-induced CNV at day 7 and 14.

(C and D) Quantification of the leakage area shown in (B) (n = 39–47 lesions from 12 to 16 eyes per group day 7; n = 11–23 lesions from 5 to 8 eyes per group for day 14).

(E) Representative confocal images of RPE-choroid flat mounts stained with CD31 and F4/80. Scale bars, 50 μm.

(F and G) Quantification of the CNV area in (E), calculated as $CD31^+$ area at the site of laser photocoagulation at day 7 and 14. (n = 15–18 lesions from 5 to 6 eyes per group for day 7; n = 11–20 lesions from 3 to 6 eyes per group for day 14).

(H and I) Quantification of the macrophages infiltration area in (E) calculated as F4/80+ area surrounding the CNV lesion at day 7 and 14. (n = 15–18 lesions from 5 to 6 eyes per group for day 7; n = 11–20 lesions from 3 to 6 eyes per group for day 14). Data are expressed as mean ± SEM, and analyzed using one-way ANOVA multiple comparisons with Tukey's method among groups in (C), (D), and (F–I) (*p < 0.05, **p < 0.01, ***p < 0.001, ****p < 0.0001).

AdC68-empty and PBS, high-dose AdC68-PFC dramatically reduced the CNV leakage area on days 7 and 14. However, treatment with a high dose of AdC68-PFC did not differ from that of conbercept (Figures 3C and 3D).

We also stained flat-mounted RPE-choroid complexes with CD31 and F4/80 on days 7 and 14 (Figure 3E). On day 7, high-dose AdC68-PFC inhibited neovascularization compared with the AdC68-empty counterpart, but low-dose AdC68-PFC and conbercept did not show an anti-angiogenic effect (Figures 3F and 3H). However, on day 14, low-dose AdC68-PFC and high-dose AdC68-PFC both showed inhibitory effects on the area of neovascularization and macrophage infiltration compared to their AdC68-empty counterparts (Figures 3G and 3I). Furthermore, compared with the PBS group, conbercept also inhibited $CD31^+$ and F4/80+ areas, which was not significantly different from the low- and high-dose AdC68-PFC groups.

These findings demonstrate that high-dose AdC68-PFC has a stronger inhibitory effect on CNV vascular leakage than low-dose AdC68-PFC does. Additionally, two doses of AdC68-PFC inhibited neovascularization and macrophage infiltration at the 14-day follow-up visit.

AdC68-PFC suppresses vascular leakage and neovascular lesions in the retina of *Vldlr*$^{-/-}$ mice model

To further assess the therapeutic effect of AdC68-PFC, another mouse model was used. Very low-density lipoprotein receptor (VLDLR)-deficient (*Vldlr*$^{-/-}$) mice develop retinal angiomatous proliferation, which is observed in 15%–20% of cases of neovascular AMD.[20,21] Elevated VEGF and inflammatory signals have been proven important for pathological subretinal angiogenesis in this model.[22] While *Vldlr*$^{-/-}$ pups develop abnormal subretinal vessels from birth, adult *Vldlr*$^{-/-}$ mice aged 6–8 weeks demonstrated sustained vascular leakage, as previously described.[23] Thus, we assessed whether the AdC68-PFC has therapeutic effects in the *Vldlr*$^{-/-}$ mouse model. We first used 6- to 8-week adult *Vldlr*$^{-/-}$ mice to explore the therapeutic effect of AdC68-PFC on vascular leakage using FFA (Figure 4A), as previously described.[23] The assessment of vascular leakage spots and vascular leakage area clearly demonstrated that 7, 14, and 35 days after IVT injection, AdC68-PFC markedly suppressed vascular leakage compared to PBS and AdC68-empty, whereas conbercept could only reduce the number of vascular leakage spots on days 7 and 14, and did not reduce the area of vascular leakage (Figures 4B–4D). These findings suggest that the AdC68-PFC was superior to conbercept, especially in long-term follow-up.

Vldlr$^{-/-}$ mice pups were used to investigate the therapeutic effect of AdC68-PFC on neovascular lesions (Figure 4E), as previously described.[22] Analysis of the total lesion number and total lesion size revealed an anti-angiogenic effect of AdC68-PFC on neovascular lesions 10 days after IVT injection, while PBS and AdC68-empty showed no effect (Figures 4F–4H). Notably, the results indicated that there was no significant difference between the AdC68-PFC and conbercept groups (Figures 4G and 4H).

AdC68-PFC inhibits VEGF-induced EC proliferation and migration *in vitro*

To further characterize endothelial cell (EC) proliferation and migration upon treatment with AdC68-PFC, 5-bromo-2-deoxyuridine and wound scratch assays were performed. The results demonstrated that compared with the control and AdC68-empty groups, AdC68-PFC showed a pronounced inhibitory effect on EC proliferation both with and without VEGF stimulation (Figures 5A and 5B). Additionally, the AdC68-PFC had an inhibitory effect on EC migration in the basal state without VEGF stimulation. After VEGF stimulation, AdC68-PFC pre-treatment showed a more robust inhibitory effect (Figures 5C and 5D). Collectively, these data suggest that the AdC68-PFC has a strong anti-angiogenic effect in ECs, especially in response to VEGF stimulation.

Suppression of VEGF-induced MAPK signal transduction pathway and LPS-induced vascular inflammation

PEDF can reportedly suppress the VEGF-VEGF receptor (VEGFR) 2 downstream mitogen-activated protein kinase (MAPK) signaling pathway under VEGF stimulation.[24] sFlt-1 binds to VEGF and involves blockade of the function of VEGF,[25] thus inhibiting the VEGF-induced MAPK signaling. Extracellular signal-regulated kinase (ERK)-MAPK signaling has been implicated in EC proliferation and motility.[26] p38 MAPK has been demonstrated to be involved in angiogenesis, migration, permeability, and survival in ECs.[27] Therefore, we evaluated the combined effect of PEDF and sFlt-1 in suppressing VEGF-induced MAPK signaling in HUVECs. According to the results, we observed that AdC68-PFC significantly reduced ERK1/2 phosphorylation in response to VEGF stimulation compared with the control group, which was much more robust than the conbercept group. In stark contrast, AdC68-PFC showed only a mild reduction, and conbercept showed no inhibitory effect without VEGF stimulation (Figures 6A and 6B). We also found that AdC68-PFC suppressed p38 MAPK phosphorylation upon VEGF

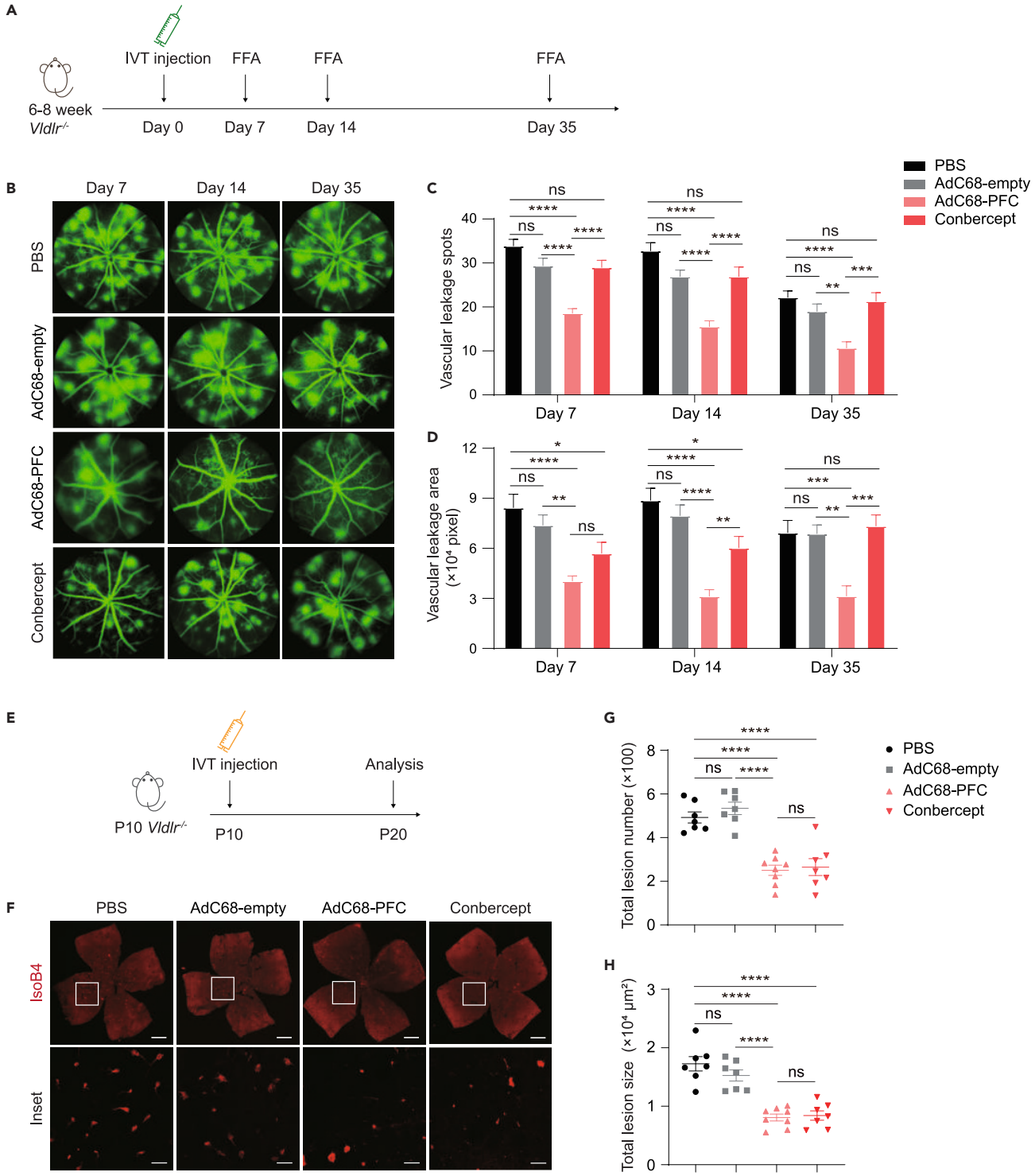

Figure 4. AdC68-PFC inhibits pathological angiogenesis in *Vldlr*$^{-/-}$ mouse model

(A) Schematic diagram illustrating the treatment strategy for adult *Vldlr*$^{-/-}$ mice in (B-D). IVT injection of PBS, AdCs (1.5×10^{9} vp), and conbercept (10 mg/mL, 1.5 μL) was performed at day 0, and FFA was performed 7, 14, and 35 days post-injection.

(B) Adult *Vldlr*$^{-/-}$ mice aged 6–8 weeks were treated as indicated. Representative FFA images show the vascular leakage from mice undergoing indicated treatment at day 7, 14, and 35.

Figure 4. *Continued*

(C and D) Quantification of the vascular leakage spots and leakage area of (B) (n = 16–19 eyes from 8 to 10 mice per group for day 7; n = 13–16 eyes from 7 to 8 mice per group for day 14; n = 10–13 eyes from 5 to 7 mice per group for day 35).

(E) Schematic diagram illustrating the treatment strategy for *Vldlr*$^{-/-}$ pups in (F–H). IVT injection of PBS, AdCs (0.8×10^9 vp), and conbercept (10 mg/mL, 0.8 μL) was performed at p10, and analysis was performed at p20.

(F) Representative confocal images of retinal flat mounts stained with IsoB4. Scale bars, 500 μm in the upper row and 50 μm in the next row.

(G and H) Quantification of the total lesion number and lesion size shown in (F) (n = 7–8 eyes from 4 to 5 mice per group). Data are expressed as mean ± SEM, and analyzed using one-way ANOVA multiple comparisons with Tukey's method among groups in (C), (D), (G), and (H) (*p < 0.05, **p < 0.01, ***p < 0.001, ****p < 0.0001). *Vldlr*$^{-/-}$, very low-density lipoprotein receptor-deficient.

stimulation, which was more robust in HUVECs pre-treated with conbercept. However, no inhibitory effects were observed in the absence of VEGF stimulation (Figures 6C and 6D).

Lipopolysaccharide (LPS) stimulation of HUVECs is commonly used as an experimental model of vascular inflammation *in vitro*. The expression of adhesion molecules, including ICAM-1 and VCAM-1, in endothelial inflammation increases robustly upon LPS stimulation.[28] PEDF downregulates the expression of ICAM-1 and VCAM-1, thus inhibiting EC leukostasis.[29–31] Similarly, we tested the combined effect of AdC68-PFC in reducing ICAM-1 and VCAM-1 with LPS stimulation. The results clearly illustrated that the AdC68-PFC showed a strong reduction compared with the control, AdC68-empty, and conbercept groups (Figures 6E–6H). Moreover, these effects were not observed in the conbercept groups, suggesting that conbercept had no clear effect on blocking LPS-induced endothelial inflammation.

AdC68-PFC does not elicit detectable adverse effects in mice

To investigate whether IVT administration of AdC68-PFC causes toxicity to the retina, we examined the morphological and structural changes in the retina 35 days after IVT injection. Optical coherence tomography was used to test the thickness of different layers of the retina, including the retinal nerve fiber ganglion cell-inner plexiform layer, inner nuclear layer, outer nuclear layer, and whole retinal thickness.[32] The results showed no significant differences between the different groups (Figures 7A–7E). Moreover, we analyzed the blood vessels of flat-mount retinas stained with CD31 (Figure 7F). The results revealed no significant differences of vascularized area between different groups (Figure 7G), suggesting that AdCs have no adverse effects on retinal vascular. Furthermore, the terminal deoxynucleotidyl transferase-mediated dUTP nick end labeling (TUNEL) assay was used to test apoptotic cells in retinas. The results suggested that TUNEL+ cells in the retina of the AdC-treated mice (both low and high dose) were not detected, which was similar to that seen in the PBS and conbercept groups (Figure 7H). In summary, these results demonstrate that AdC68-PFC is not significantly toxic.

DISCUSSION

In this study, we constructed a recombinant AdC and assessed its expression, efficacy, and safety. Our results showed that the AdC68-PFC that we generated can efficiently mediate gene expression of PEDF, sFlt-1, and sCD59 both *in vitro* and *in vivo*. Moreover, AdC68-PFC has been proven safe, tolerable, and efficient at suppressing vascular leakage, neovascularization, and inflammation in laser-induced CNV and *Vldlr*$^{-/-}$ animal models, and demonstrated a suppressive effect on EC proliferation, migration, and inflammation.

Due to the limited efficacy of anti-VEGF monotherapy in treating nAMD, several multitarget drugs have been developed, such as faricimab and efdamrofusp alfa. These drugs target VEGFA/angiopoietin-2 and the complement cascade/VEGF family, respectively. Their success highlights the potential therapeutic benefits of multitarget approaches for nAMD. Given that choroidal inflammation and complement activation are prominent features of AMD, we have selected PEDF and sCD59, in addition to the VEGF neutralizing protein sFlt-1, as our target genes.[33,34] PEDF is a 50-kDa multifunctional glycoprotein belonging to the serine protease inhibitor (serpins) family. It has demonstrated suppressive effects on angiogenesis, inflammation, and fibrosis.[35] A clinical trial by Campochiaro et al. utilized an adenoviral vector encoding PEDF as a single gene therapy for nAMD (NCT00109499). The results indicated the safety and tolerability of IVT injection of the adenoviral vector expressing human PEDF. Patients receiving a lower dose of less than 10^8 particle units experienced visual impairment and an enlargement of the CNV lesion area, while those receiving 10^8 or more particle units remained stable, suggesting a potential dose-escalation response.[36] Subsequent clinical and preclinical studies have further demonstrated the efficacy of PEDF as a single or multiple gene therapy for nAMD.[37–39] sFlt-1 is an endogenously expressed VEGF antagonist that binds to and neutralizes VEGFA, thereby preventing the normal binding of VEGF to its endothelial receptors.[40] Preclinical studies have demonstrated the mechanism of gene therapy using sFlt-1 to inhibit CNV formation.[41,42] Phase I and Phase II clinical trials have also investigated the safety profile and effectiveness of subretinal injections of rAAV-sFlt-1 in human nAMD (NCT01494805, NCT01024998). CD59 is a naturally occurring membrane-bound inhibitor of MAC formation, which binds to the terminal complement protein complex C5b-8, thereby preventing the incorporation of C9 molecules required to complete the formation of pores on cell membranes.[43] MAC-mediated release of growth factors, including β-fibroblast growth factor and VEGF, may be a pathogenic mechanism in angiogenesis.[44,45] Moreover, a recent study suggested that the inhibition of MAC deposition and complement activation is related to decreased F4/80+ macrophage infiltration and could further suppress CNV progression. The sCD59 delivered via a gene therapy approach using adenoviral and AAV vectors has been demonstrated to attenuate MAC deposition and CNV in the eyes of mice.[46,47] The preclinical effectiveness has encouraged Hemera Biosciences to construct an AAVCAGsCD59 (HMR59) gene therapy vector for the treatment of human dry AMD (NCT03144999).

In our study, we took advantage of the large capacity of AdCs and inserted three genes in the E1 area of AdCs simultaneously, with the cleavable linker P2A to ensure the separate expression of the therapeutic genes. The recombinant AdC that we generated had a dual and

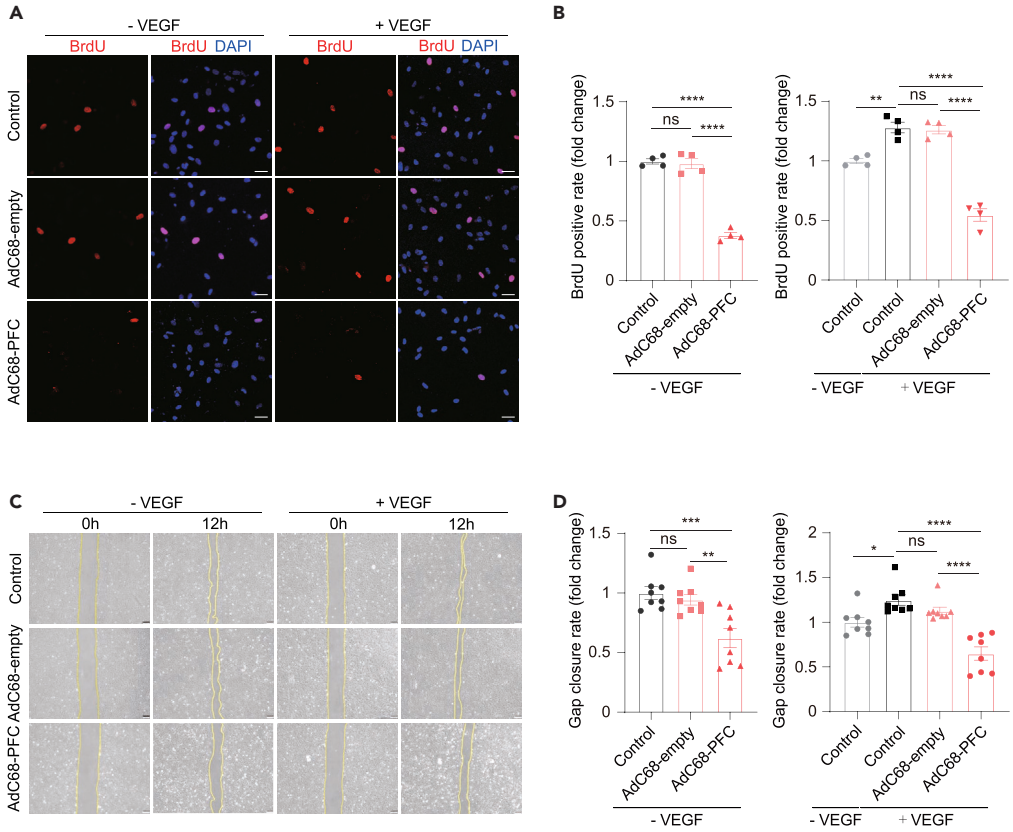

Figure 5. AdC68-PFC suppresses vascular proliferation and migration *in vitro*

(A) Starved HUVECs were pre-treated with AdC68-empty (2.5×10^9 vp) and AdC68-PFC (2.5×10^9 vp) for 24 h and then stimulated with 50 ng/mL VEGF for 24 h. Representative images showing the immunostaining results of BrdU indicate the proliferation of HUVECs. Scale bars, 50 μm.

(B) Quantification of the percentages of BrdU+DAPI+ cells in DAPI+ cells (n = 4 biological repeats) shown in (A), and the results were normalized to the control condition.

(C and D) Starved HUVECs were pre-treated with AdC68-empty (1×10^{10} vp) and AdC68-PFC (1×10^{10} vp) for 48 h and then stimulated with 50 ng/mL VEGF for 12 h. Representative images showing wound-healing scratch experiments and the gap closure rate was calculated (D) (n = 8 biological repeats). The results were normalized to the control condition. Scale bars, 50 μm. Data are expressed as mean ± SEM, and analyzed using one-way ANOVA multiple comparisons with Tukey's method among groups in (B) and (D) (*p < 0.05, **p < 0.01, ***p < 0.001, ****p < 0.0001). HUVEC, Human Umbilical Vascular Endothelial Cell.

strong inhibitory effect on pathological vascularization and inflammation. This has not been performed before because of the limited packaging capacity of AAV.[48] Although AAV vectors are now the most popular viral vectors for gene therapy owing to their long-lasting gene expression, low inflammatory response, and low immunogenicity, there are still challenges in the application of AAV vectors. For instance, in addition to the limited transgene capacity mentioned previously, there is the difficulty of mass production of AAV, which leads to high treatment costs.[49] Therefore, AAV vectors may not be suitable for simultaneously carrying PEDF, sFlt-1, and sCD59. By contrast, adenoviral vectors are more appropriate for our study. Notably, adenoviral vectors reportedly activate the innate immune response, which is a major obstacle in the application of these agents in human gene therapy.[50,51] However, the presence of the blood-retinal barrier and the combination of heterologous adenoviral vectors might help ignore the influence of the negative immune response induced by the vector itself.

Although this study focused on CNV, it would also be interesting to test the efficacy of AdC68-PFC in other disease models of pathological angiogenesis. Of note, the oxygen-induced retinopathy (OIR) mouse model, which is the most widely used model for retinal neovascularization and inflammation, has also been demonstrated in the OIR pathogenesis.[52,53] OIR model resembles human retinopathy of prematurity, proliferative diabetic retinopathy, and retinal vein occlusion.[54,55] As our results showed that AdC68-PFC inhibited vascular leakage and neovascularization, and suppressed macrophage infiltration in laser-induced CNV models, further studies are required to test the therapeutic effect of AdC68-PFC in the OIR model. Corneal neovascularization (CoNV) is a sight-threatening disease that is usually related to inflammatory disorders of the ocular surface.[56–58] Similarly, AdC68-PFC can also be applied for the treatment of CoNV.

In summary, AdC68-PFC provided sustained delivery of anti-angiogenic and anti-inflammatory proteins following IVT injection, leading to efficacious inhibition of CNV for up to 35 days. This study reuses adenoviral vectors for gene therapy strategy, and we conducted a comprehensive efficacy evaluation in both laser-induced CNV and *Vldlr*$^{-/-}$ mouse models and further assessed their anti-vascular and

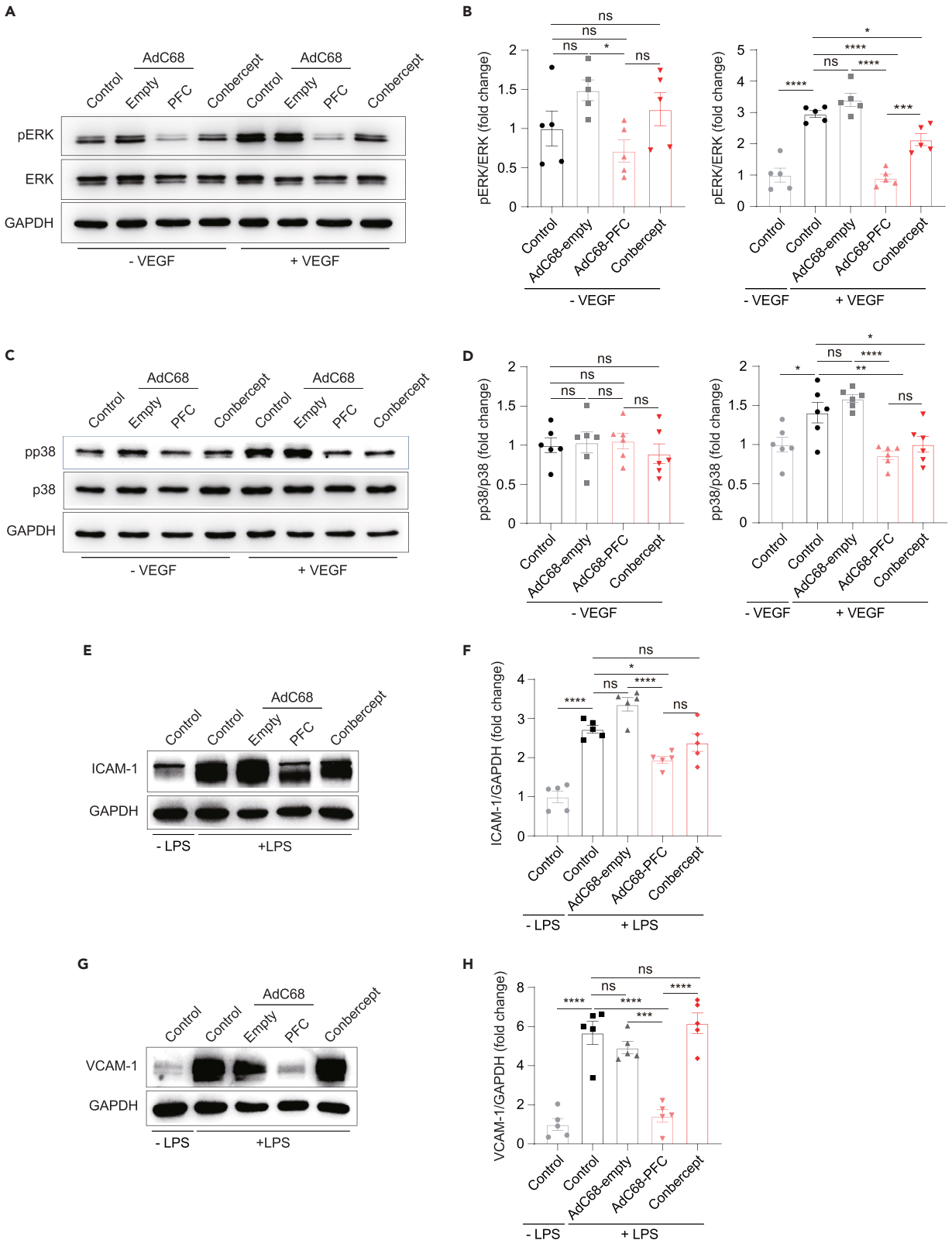
A
AdC68
Control
Empty
PFC
Conbercept
Control
Empty
PFC
Conbercept
pERK
ERK
GAPDH
- VEGF
+ VEGF
B
pERK/ERK (fold change)
ns
ns
ns
*
ns
****
***
Control
AdC68-empty
AdC68-PFC
Conbercept
- VEGF
+ VEGF
C
pp38
p38
GAPDH
D
pp38/p38 (fold change)
**
E
ICAM-1
- LPS
+LPS
F
ICAM-1/GAPDH (fold change)
G
VCAM-1
H
VCAM-1/GAPDH (fold change)

Figure 6. AdC68-PFC suppresses VEGF-induced MAPK signal transduction pathway and LPS-induced vascular inflammation in ECs

(A) Starved HUVECs were pre-treated with AdC68-empty (1×10^{10} vp), AdC68-PFC (1×10^{10} vp) for 48 h and then stimulated with 50 ng/mL VEGF for 10 min. Conbercept (10 μg) was used as a positive control, and the pre-treatment time was 5 min before VEGF stimulation. Representative western blot show pERK and total ERK expression in HUVECs.

(B) Quantification of pERK/total ERK (n = 5 biological repeats) shown in (A).

(C and D) Western blot analysis of pp38 and total p38 in HUVECs treated as in (A) and quantification (n = 6 biological repeats).

(E) Starved HUVECs were pre-treated with AdC68-empty (1×10^{10} vp), AdC68-PFC (1×10^{10} vp) for 40 h and then stimulated with LPS (1 μg/mL) for 8 h. Conbercept (10 μg) was used as a positive control, and the pre-treatment time was 5 min after LPS stimulation. Representative western blot for ICAM-1 expression in HUVECs.

(F) Quantification of ICAM-1 (n = 5 biological repeats) shown in (E).

(G and H) Western blot analysis of VCAM-1 in HUVECs treated as in (E) and quantification (n = 5 biological repeats). Data are expressed as mean ± SEM, and analyzed using one-way ANOVA multiple comparisons with Tukey's method among groups in (B), (D), (F), and (H) (*$p < 0.05$, **$p < 0.01$, ***$p < 0.001$, ****$p < 0.0001$). VEGF, vascular endothelial-derived growth factor; MAPK, mitogen-activated protein kinase. LPS, lipopolysaccharides; EC, endothelial cell.

anti-inflammatory effects in ECs. The results of our study encourage us to study helper-dependent adenovirus (HDAd) vectors, which may be a potential long-acting and relatively safe gene therapy vector for the treatment of eye diseases in the future.

Limitations of the study

There are three main limitations of this study. First, in our study, we used a rodent animal model instead of primates. C57BL/6J mice do not have maculae, and acute injury-related angiogenesis and inflammation in the laser-induced CNV model fundamentally differ from the genetically influenced, long-standing senescent degeneration and chronic pathology of AMD. Second, the transgene expression time of AdCs is relatively shorter compared to AAV vectors, lasting only approximately 35 days. For clinical use in the future, new AdCs and long-term assessment of toxicity are required. Thus, it would be valuable to explore the use of HDAd vectors, which offer a larger DNA-carrying capacity, longer term transgene expression, and reduced toxicity.[59,60] Third, while our *in vivo* data demonstrate that eGFP expression driven by the cytomegalovirus (CMV) promoter can persist for approximately 35 days, it is important to note that the CMV promoter is susceptible to transcriptional silencing, potentially due to CpG island methylation within the CMV promoter.[61] To overcome this limitation, alternative promoters should be considered for achieving stable transgene expression. One example is the CAG promoter, which combines the CMV enhancer with the chicken beta-actin promoter and has been shown to be a robust and stable artificial construct.[62]

STAR★METHODS

Detailed methods are provided in the online version of this paper and include the following:

- KEY RESOURCES TABLE
- RESOURCE AVAILABILITY
  - Lead contact
  - Materials availability
  - Data and code availability
- EXPERIMENTAL MODEL AND STUDY PARTICIPANT DETAILS
  - Animals
  - Laser-induced CNV model
  - Cell cultures
- METHOD DETAILS
  - Vector production
  - PEDF, sFlt-1, and sCD59 expression analyses
  - IVT injection
  - *In vivo* fluorescence imaging
  - FFA
  - Immunofluorescence
  - Western blot assay
  - RNA extraction, complementary DNA synthesis, and quantitative real-time qPCR analysis
  - The BrdU incorporation assay in ECs
  - Scratch assay
  - OCT
  - TUNEL assay
- QUANTIFICATION AND STATISTICAL ANALYSIS

SUPPLEMENTAL INFORMATION

Supplemental information can be found online at https://doi.org/10.1016/j.isci.2023.107939.

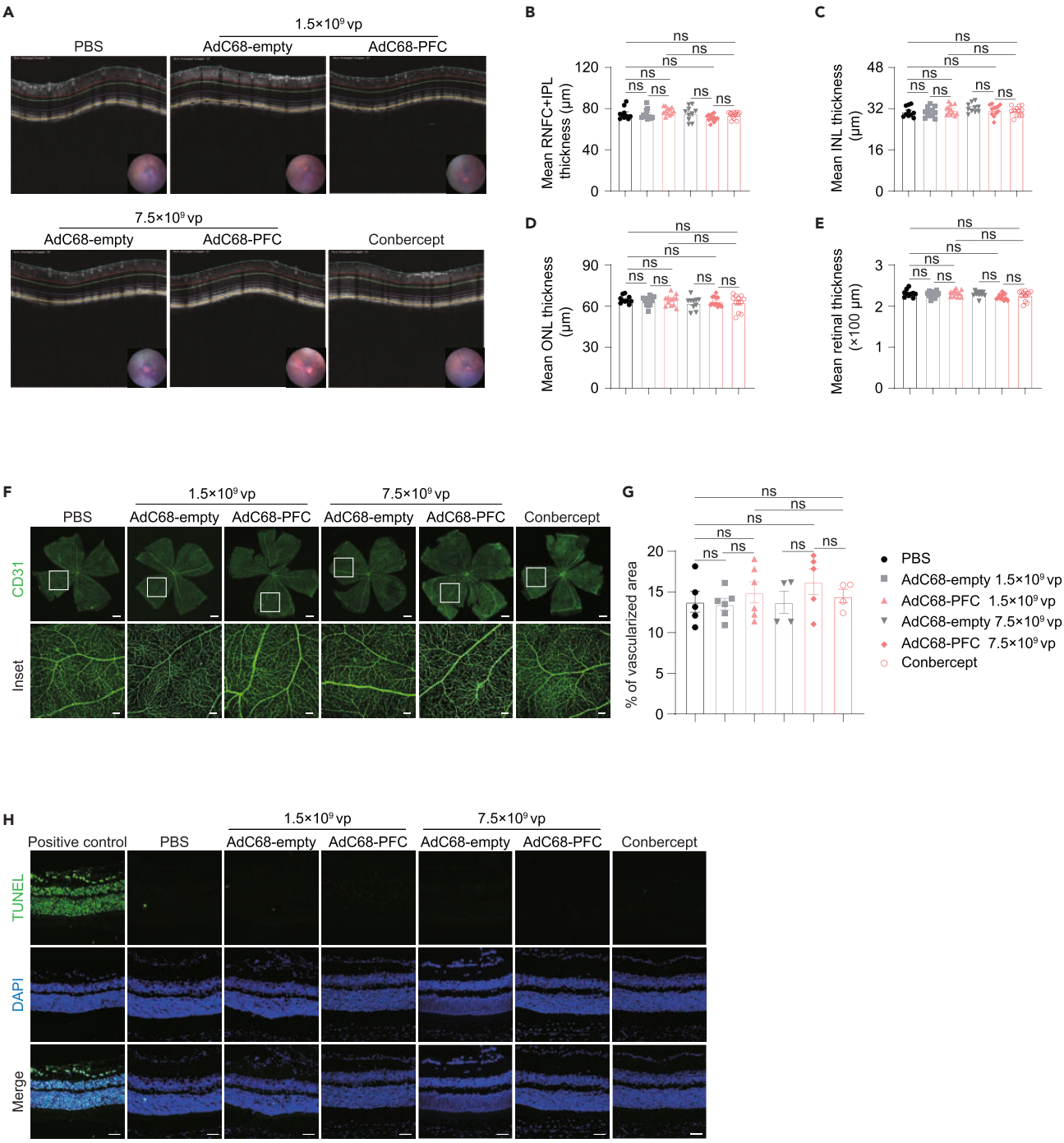

Figure 7. Safety test following AdC68-PFC intraocular injection

(A) The retina thickness 35 days after IVT injection of PBS, AdC68-empty, AdC68-PFC, or conbercept was visualized by OCT.

(B–E) Quantification of (B) RNFGC-IPL (n = 10–12 eyes from 5 to 6 mice per group), (C) INL (n = 10–12 eyes from 5 to 6 mice per group), (D) ONL (n = 10–12 eyes from 5 to 6 mice per group) and (E) retina (n = 10–12 eyes from 5 to 6 mice per group) 35 days after IVT injection.

(F) Representative confocal images of retinal flat mounts stained with CD31. Scale bars, 500 μm in the upper row and 100 μm in the next row.

(G) Quantification of % of vascularized area shown in (F) (n = 4–6 eyes from 4 to 6 mice per group).

(H) Representative confocal images show TUNEL$^+$ cells (TUNEL, green) in the retina. Scale bars, 50 μm. Data are expressed as mean ± SEM, and analyzed using one-way ANOVA multiple comparisons with Tukey's method among groups in (B), (C), (D), (E), and (G). (*$p < 0.05$, **$p < 0.01$, ***$p < 0.001$, ****$p < 0.0001$). OCT, optical coherence tomography; RNFGC-IPL, retinal nerve fiber ganglion cell-inner plexiform layer; INL, inner nuclear layer; ONL, outer nuclear layer.

ACKNOWLEDGMENTS

This work was supported by the National Key Research and Development Program of China (2021YFC2401404) and the National Natural Science Foundation of China (82020108007, 81830026) to H.Y., and supported by the National Natural Science Foundation of China (32070926) and the Key Project of the Natural Science Foundation of Tianjin (20JCZDJC00090) to D.Z.

AUTHOR CONTRIBUTIONS

H.Y., D.Z., and X.W. conceived the project and designed the experiments. S.Z., B.C., M.X., J.L., K.H., Y.L., X.D., T.B., W.Z., H.Z., and S.L. performed the experiments. H.Y., D.Z., X.W., and S.Z. analyzed the data. S.Z. and B.C. wrote the manuscript. H.Y., D.Z., and X.W. revised the manuscript.

DECLARATION OF INTERESTS

All authors declare no competing interests.

INCLUSION AND DIVERSITY

We support inclusive, diverse, and equitable conduct of the research.

Received: January 4, 2023
Revised: June 9, 2023
Accepted: September 13, 2023
Published: September 16, 2023

REFERENCES

1. Thomas, C.J., Mirza, R.G., and Gill, M.K. (2021). Age-Related Macular Degeneration. Med. Clin. *105*, 473–491. https://doi.org/10.1016/j.mcna.2021.01.003.
2. Mitchell, P., Liew, G., Gopinath, B., and Wong, T.Y. (2018). Age-related macular degeneration. Lancet *392*, 1147–1159. https://doi.org/10.1016/s0140-6736(18)31550-2.
3. Flores, R., Carneiro, Â., Vieira, M., Tenreiro, S., and Seabra, M.C. (2021). Age-Related Macular Degeneration: Pathophysiology, Management, and Future Perspectives. Ophthalmologica *244*, 495–511. https://doi.org/10.1159/000517520.
4. Stahl, A. (2020). The Diagnosis and Treatment of Age-Related Macular Degeneration. Dtsch. Arztebl. Int. *117*, 513–520. https://doi.org/10.3238/arztebl.2020.0513.
5. Solomon, S.D., Lindsley, K., Vedula, S.S., Krzystolik, M.G., and Hawkins, B.S. (2019). Anti-vascular endothelial growth factor for neovascular age-related macular degeneration. Cochrane Database Syst. Rev. *3*, Cd005139. https://doi.org/10.1002/14651858.CD005139.pub4.
6. Gillies, M.C., Daien, V., Nguyen, V., and Barthelmes, D. (2017). Re: Comparison of Age-Related Macular Degeneration Treatments Trials (CATT) Research Group, et al.: Five-year outcomes with anti-vascular endothelial growth factor treatment of neovascular age-related macular degeneration: The Comparison of Age-Related Macular Degeneration Treatments Trials (Ophthalmology 2016;123:1751-1761). Ophthalmology *124*, e31–e32. https://doi.org/10.1016/j.ophtha.2016.05.054.
7. Rofagha, S., Bhisitkul, R.B., Boyer, D.S., Sadda, S.R., and Zhang, K.; SEVEN-UP Study Group (2013). Seven-year outcomes in ranibizumab-treated patients in ANCHOR, MARINA, and HORIZON: a multicenter cohort study (SEVEN-UP). Ophthalmology *120*, 2292–2299. https://doi.org/10.1016/j.ophtha.2013.03.046.
8. van Lookeren Campagne, M., LeCouter, J., Yaspan, B.L., and Ye, W. (2014). Mechanisms of age-related macular degeneration and therapeutic opportunities. J. Pathol. *232*, 151–164. https://doi.org/10.1002/path.4266.
9. Yang, S., Li, T., Jia, H., Gao, M., Li, Y., Wan, X., Huang, Z., Li, M., Zhai, Y., Li, X., et al. (2022). Targeting C3b/C4b and VEGF with a bispecific fusion protein optimized for neovascular age-related macular degeneration therapy. Sci. Transl. Med. *14*, eabj2177. https://doi.org/10.1126/scitranslmed.abj2177.
10. Ding, K., Eaton, L., Bowley, D., Rieser, M., Chang, Q., Harris, M.C., Clabbers, A., Dong, F., Shen, J., Hackett, S.F., et al. (2017). Generation and characterization of ABBV642, a dual variable domain immunoglobulin molecule (DVD-Ig) that potently neutralizes VEGF and PDGF-BB and is designed for the treatment of exudative age-related macular degeneration. mAbs *9*, 269–284. https://doi.org/10.1080/19420862.2016.1268305.
11. Nicolò, M., Ferro Desideri, L., Vagge, A., and Traverso, C.E. (2021). Faricimab: an investigational agent targeting the Tie-2/angiopoietin pathway and VEGF-A for the treatment of retinal diseases. Expet Opin. Invest. Drugs *30*, 193–200. https://doi.org/10.1080/13543784.2021.1879791.
12. Kumaran, N., Michaelides, M., Smith, A.J., Ali, R.R., and Bainbridge, J.W.B. (2018). Retinal gene therapy. Br. Med. Bull. *126*, 13–25. https://doi.org/10.1093/bmb/ldy005.
13. Guimaraes, T.A.C.d., Georgiou, M., Bainbridge, J.W.B., and Michaelides, M. (2021). Gene therapy for neovascular age-related macular degeneration: rationale, clinical trials and future directions. Br. J. Ophthalmol. *105*, 151–157. https://doi.org/10.1136/bjophthalmol-2020-316195.
14. Guo, J., Mondal, M., and Zhou, D. (2018). Development of novel vaccine vectors: Chimpanzee adenoviral vectors. Hum. Vaccines Immunother. *14*, 1679–1685. https://doi.org/10.1080/21645515.2017.1419108.
15. Chng, J., Wang, T., Nian, R., Lau, A., Hoi, K.M., Ho, S.C.L., Gagnon, P., Bi, X., and Yang, Y. (2015). Cleavage efficient 2A peptides for high level monoclonal antibody expression in CHO cells. mAbs *7*, 403–412. https://doi.org/10.1080/19420862.2015.1008351.
16. Mori, K., Duh, E., Gehlbach, P., Ando, A., Takahashi, K., Pearlman, J., Mori, K., Yang, H.S., Zack, D.J., Ettyreddy, D., et al. (2001). Pigment epithelium-derived factor inhibits retinal and choroidal neovascularization. J. Cell. Physiol. *188*, 253–263. https://doi.org/10.1002/jcp.1114.
17. Xu, Y., Cui, K., Li, J., Tang, X., Lin, J., Lu, X., Huang, R., Yang, B., Shi, Y., Ye, D., et al. (2020). Melatonin attenuates choroidal neovascularization by regulating macrophage/microglia polarization via inhibition of RhoA/ROCK signaling pathway. J. Pineal Res. *69*, e12660. https://doi.org/10.1111/jpi.12660.
18. Ivanescu, A.A., Fernández-Robredo, P., Heras-Mulero, H., Sádaba-Echarri, L.M., García-García, L., Fernández-García, V., Moreno-Orduna, M., Redondo-Exposito, A., Recalde, S., and García-Layana, A. (2015). Modifying Choroidal Neovascularization Development with a Nutritional Supplement in Mice. Nutrients *7*, 5423–5442. https://doi.org/10.3390/nu7075229.
19. Pennesi, M.E., Neuringer, M., and Courtney, R.J. (2012). Animal models of age related macular degeneration. Mol. Aspect. Med. *33*, 487–509. https://doi.org/10.1016/j.mam.2012.06.003.
20. Fu, Z., Liegl, R., Wang, Z., Gong, Y., Liu, C.H., Sun, Y., Cakir, B., Burnim, S.B., Meng, S.S., Löfqvist, C., et al. (2017). Adiponectin Mediates Dietary Omega-3 Long-Chain Polyunsaturated Fatty Acid Protection Against Choroidal Neovascularization in

Mice. Invest. Ophthalmol. Vis. Sci. *58*, 3862–3870. https://doi.org/10.1167/iovs.17-21796.
21. Joyal, J.S., Sun, Y., Gantner, M.L., Shao, Z., Evans, L.P., Saba, N., Fredrick, T., Burnim, S., Kim, J.S., Patel, G., et al. (2016). Retinal lipid and glucose metabolism dictates angiogenesis through the lipid sensor Ffar1. Nat. Med. *22*, 439–445. https://doi.org/10.1038/nm.4059.
22. Sun, Y., Lin, Z., Liu, C.H., Gong, Y., Liegl, R., Fredrick, T.W., Meng, S.S., Burnim, S.B., Wang, Z., Akula, J.D., et al. (2017). Inflammatory signals from photoreceptor modulate pathological retinal angiogenesis via c-Fos. J. Exp. Med. *214*, 1753–1767. https://doi.org/10.1084/jem.20161645.
23. Huang, L., Liang, W., Zhou, K., Wassel, R.A., Ridge, Z.D., Ma, J.X., and Wang, B. (2021). Therapeutic Effects of Fenofibrate Nano-Emulsion Eye Drops on Retinal Vascular Leakage and Neovascularization. Biology *10*, 1328. https://doi.org/10.3390/biology10121328.
24. Yang, J., Duh, E.J., Caldwell, R.B., and Behzadian, M.A. (2010). Antipermeability function of PEDF involves blockade of the MAP kinase/GSK/beta-catenin signaling pathway and uPAR expression. Invest. Ophthalmol. Vis. Sci. *51*, 3273–3280. https://doi.org/10.1167/iovs.08-2878.
25. Levine, R.J., Maynard, S.E., Qian, C., Lim, K.H., England, L.J., Yu, K.F., Schisterman, E.F., Thadhani, R., Sachs, B.P., Epstein, F.H., et al. (2004). Circulating angiogenic factors and the risk of preeclampsia. N. Engl. J. Med. *350*, 672–683. https://doi.org/10.1056/NEJMoa031884.
26. Mavria, G., Vercoulen, Y., Yeo, M., Paterson, H., Karasarides, M., Marais, R., Bird, D., and Marshall, C.J. (2006). ERK-MAPK signaling opposes Rho-kinase to promote endothelial cell survival and sprouting during angiogenesis. Cancer Cell *9*, 33–44. https://doi.org/10.1016/j.ccr.2005.12.021.
27. Simons, M., Gordon, E., and Claesson-Welsh, L. (2016). Mechanisms and regulation of endothelial VEGF receptor signalling. Nat. Rev. Mol. Cell Biol. *17*, 611–625. https://doi.org/10.1038/nrm.2016.87.
28. Hou, X., Yang, S., and Yin, J. (2019). Blocking the REDD1/TXNIP axis ameliorates LPS-induced vascular endothelial cell injury through repressing oxidative stress and apoptosis. Am. J. Physiol. Cell Physiol. *316*. C104-c110. https://doi.org/10.1152/ajpcell.00313.2018.
29. Falero-Perez, J., Park, S., Sorenson, C.M., and Sheibani, N. (2017). PEDF expression affects retinal endothelial cell proangiogenic properties through alterations in cell adhesive mechanisms. Am. J. Physiol. Cell Physiol. *313*. C405-c420. https://doi.org/10.1152/ajpcell.00004.2017.
30. Michalczyk, E.R., Chen, L., Fine, D., Zhao, Y., Mascarinas, E., Grippo, P.J., and DiPietro, L.A. (2018). Pigment Epithelium-Derived Factor (PEDF) as a Regulator of Wound Angiogenesis. Sci. Rep. *8*, 11142. https://doi.org/10.1038/s41598-018-29465-9.
31. Zhang, S.X., Wang, J.J., Gao, G., Shao, C., Mott, R., and Ma, J.X. (2006). Pigment epithelium-derived factor (PEDF) is an endogenous antiinflammatory factor. Faseb. J. *20*, 323–325. https://doi.org/10.1096/fj.05-4313fje.
32. Dysli, C., Enzmann, V., Sznitman, R., and Zinkernagel, M.S. (2015). Quantitative Analysis of Mouse Retinal Layers Using Automated Segmentation of Spectral Domain Optical Coherence Tomography Images. Transl. Vis. Sci. Technol. *4*, 9. https://doi.org/10.1167/tvst.4.4.9.
33. Hachana, S., Fontaine, O., Sapieha, P., Lesk, M., Couture, R., and Vaucher, E. (2020). The effects of anti-VEGF and kinin B(1) receptor blockade on retinal inflammation in laser-induced choroidal neovascularization. Br. J. Pharmacol. *177*, 1949–1966. https://doi.org/10.1111/bph.14962.
34. Ricci, F., Bandello, F., Navarra, P., Staurenghi, G., Stumpp, M., and Zarbin, M. (2020). Neovascular Age-Related Macular Degeneration: Therapeutic Management and New-Upcoming Approaches. Int. J. Mol. Sci. *21*, 8242. https://doi.org/10.3390/ijms21218242.
35. Farnoodian, M., Sorenson, C.M., and Sheibani, N. (2018). PEDF expression affects the oxidative and inflammatory state of choroidal endothelial cells. Am. J. Physiol. Cell Physiol. *314*. C456-c472. https://doi.org/10.1152/ajpcell.00259.2017.
36. Campochiaro, P.A., Nguyen, Q.D., Shah, S.M., Klein, M.L., Holz, E., Frank, R.N., Saperstein, D.A., Gupta, A., Stout, J.T., Macko, J., et al. (2006). Adenoviral vector-delivered pigment epithelium-derived factor for neovascular age-related macular degeneration: results of a phase I clinical trial. Hum. Gene Ther. *17*, 167–176. https://doi.org/10.1089/hum.2006.17.167.
37. Askou, A.L., Alsing, S., Benckendorff, J.N.E., Holmgaard, A., Mikkelsen, J.G., Aagaard, L., Bek, T., and Corydon, T.J. (2019). Suppression of Choroidal Neovascularization by AAV-Based Dual-Acting Antiangiogenic Gene Therapy. Mol. Ther. Nucleic Acids *16*, 38–50. https://doi.org/10.1016/j.omtn.2019.01.012.
38. Askou, A.L., and Corydon, T.J. (2018). Development of Multigenic Lentiviral Vectors for Cell-Specific Expression of Antiangiogenic miRNAs and Protein Factors. Methods Mol. Biol. *1715*, 47–60. https://doi.org/10.1007/978-1-4939-7522-8_4.
39. Hamilton, M.M., Byrnes, G.A., Gall, J.G., Brough, D.E., King, C.R., and Wei, L.L. (2008). Alternate serotype adenovector provides long-term therapeutic gene expression in the eye. Mol. Vis. *14*, 2535–2546.
40. Luo, L., Uehara, H., Zhang, X., Das, S.K., Olsen, T., Holt, D., Simonis, J.M., Jackman, K., Singh, N., Miya, T.R., et al. (2013). Photoreceptor avascular privilege is shielded by soluble VEGF receptor-1. Elife *2*, e00324. https://doi.org/10.7554/eLife.00324.
41. Murakami, Y., Ikeda, Y., Yonemitsu, Y., Miyazaki, M., Inoue, M., Hasegawa, M., Sueishi, K., and Ishibashi, T. (2010). Inhibition of choroidal neovascularization via brief subretinal exposure to a newly developed lentiviral vector pseudotyped with Sendai viral envelope proteins. Hum. Gene Ther. *21*, 199–209. https://doi.org/10.1089/hum.2009.102.
42. Igarashi, T., Miyake, K., Masuda, I., Takahashi, H., and Shimada, T. (2010). Adeno-associated vector (type 8)-mediated expression of soluble Flt-1 efficiently inhibits neovascularization in a murine choroidal neovascularization model. Hum. Gene Ther. *21*, 631–637. https://doi.org/10.1089/hum.2009.153.
43. Rollins, S.A., and Sims, P.J. (1990). The complement-inhibitory activity of CD59 resides in its capacity to block incorporation of C9 into membrane C5b-9. J. Immunol. *144*, 3478–3483.
44. Bora, P.S., Sohn, J.H., Cruz, J.M.C., Jha, P., Nishihori, H., Wang, Y., Kaliappan, S., Kaplan, H.J., and Bora, N.S. (2005). Role of complement and complement membrane attack complex in laser-induced choroidal neovascularization. J. Immunol. *174*, 491–497. https://doi.org/10.4049/jimmunol.174.1.491.
45. Liu, J., Jha, P., Lyzogubov, V.V., Tytarenko, R.G., Bora, N.S., and Bora, P.S. (2011). Relationship between complement membrane attack complex, chemokine (C-C motif) ligand 2 (CCL2) and vascular endothelial growth factor in mouse model of laser-induced choroidal neovascularization. J. Biol. Chem. *286*, 20991–21001. https://doi.org/10.1074/jbc.M111.226266.
46. Adhi, M., Cashman, S.M., and Kumar-Singh, R. (2013). Adeno-associated virus mediated delivery of a non-membrane targeted human soluble CD59 attenuates some aspects of diabetic retinopathy in mice. PLoS One *8*, e79661. https://doi.org/10.1371/journal.pone.0079661.
47. Cashman, S.M., Ramo, K., and Kumar-Singh, R. (2011). A non membrane-targeted human soluble CD59 attenuates choroidal neovascularization in a model of age related macular degeneration. PLoS One *6*, e19078. https://doi.org/10.1371/journal.pone.0019078.
48. Wang, T., Zhu, X., Yi, H., Gu, J., Liu, S., Izenwasser, S., Lemmon, V.P., Roy, S., and Hao, S. (2021). Viral vector-mediated gene therapy for opioid use disorders. Exp. Neurol. *341*, 113710. https://doi.org/10.1016/j.expneurol.2021.113710.
49. Bulcha, J.T., Wang, Y., Ma, H., Tai, P.W.L., and Gao, G. (2021). Viral vector platforms within the gene therapy landscape. Signal Transduct. Targeted Ther. *6*, 53. https://doi.org/10.1038/s41392-021-00487-6.
50. Greber, U.F., and Flatt, J.W. (2019). Adenovirus Entry: From Infection to Immunity. Annu. Rev. Virol. *6*, 177–197. https://doi.org/10.1146/annurev-virology-092818-015550.
51. Muruve, D.A. (2004). The innate immune response to adenovirus vectors. Hum. Gene Ther. *15*, 1157–1166. https://doi.org/10.1089/hum.2004.15.1157.
52. Rojo Arias, J.E., Englmaier, V.E., and Jászai, J. (2022). VEGF-Trap Modulates Retinal Inflammation in the Murine Oxygen-Induced Retinopathy (OIR) Model. Biomedicines *10*, 201. https://doi.org/10.3390/biomedicines10020201.
53. Li, J., Yu, S., Lu, X., Cui, K., Tang, X., Xu, Y., and Liang, X. (2021). The phase changes of M1/M2 phenotype of microglia/macrophage following oxygen-induced retinopathy in mice. Inflamm. Res. *70*, 183–192. https://doi.org/10.1007/s00011-020-01427-w.
54. Scott, A., and Fruttiger, M. (2010). Oxygen-induced retinopathy: a model for vascular pathology in the retina. Eye *24*, 416–421. https://doi.org/10.1038/eye.2009.306.
55. Vähätupa, M., Järvinen, T.A.H., and Uusitalo-Järvinen, H. (2020). Exploration of Oxygen-Induced Retinopathy Model to Discover New Therapeutic Drug Targets in Retinopathies. Front. Pharmacol. *11*, 873. https://doi.org/10.3389/fphar.2020.00873.
56. Chang, J.H., Gabison, E.E., Kato, T., and Azar, D.T. (2001). Corneal neovascularization. Curr. Opin. Ophthalmol. *12*, 242–249. https://doi.org/10.1097/00055735-200108000-00002.
57. Nicholas, M.P., and Mysore, N. (2021). Corneal neovascularization. Exp. Eye Res.

202, 108363. https://doi.org/10.1016/j.exer.2020.108363.

58. Barry, Z., Park, B., and Corson, T.W. (2020). Pharmacological Potential of Small Molecules for Treating Corneal Neovascularization. Molecules *25*, 3468. https://doi.org/10.3390/molecules25153468.
59. Bandara, R.A., Chen, Z.R., and Hu, J. (2021). Potential of helper-dependent Adenoviral vectors in CRISPR-cas9-mediated lung gene therapy. Cell Biosci. *11*, 145. https://doi.org/10.1186/s13578-021-00662-w.
60. Cots, D., Bosch, A., and Chillón, M. (2013). Helper dependent adenovirus vectors: progress and future prospects. Curr. Gene Ther. *13*, 370–381. https://doi.org/10.2174/15665232130513121212533 8.
61. Zúñiga, R.A., Gutiérrez-González, M., Collazo, N., Sotelo, P.H., Ribeiro, C.H., Altamirano, C., Lorenzo, C., Aguillón, J.C., and Molina, M.C. (2019). Development of a new promoter to avoid the silencing of genes in the production of recombinant antibodies in chinese hamster ovary cells. J. Biol. Eng. *13*, 59. https://doi.org/10.1186/s13036-019-0187-y.
62. Farokhimanesh, S., Rahbarizadeh, F., Rasaee, M.J., Kamali, A., and Mashkani, B. (2010). Hybrid promoters directed tBid gene expression to breast cancer cells by transcriptional targeting. Biotechnol. Prog. *26*, 505–511. https://doi.org/10.1002/btpr.353.
63. Fu, Y., Hou, Y., Fu, C., Gu, M., Li, C., Kong, W., Wang, X., Shyy, J.Y.J., and Zhu, Y. (2011). A novel mechanism of gamma/delta T-lymphocyte and endothelial activation by shear stress: the role of ecto-ATP synthase beta chain. Circ. Res. *108*, 410–417. https://doi.org/10.1161/CIRCRESAHA.110.230151.
64. Yang, Y., Chi, Y., Tang, X., Ertl, H.C., and Zhou, D. (2016). Rapid, Efficient, and Modular Generation of Adenoviral Vectors via Isothermal Assembly. Curr. Protoc. Mol. Biol. *113*, 16–26. https://doi.org/10.1002/0471142727.mb1626s113.
65. Zhou, D., Zhou, X., Bian, A., Li, H., Chen, H., Small, J.C., Li, Y., Giles-Davis, W., Xiang, Z., and Ertl, H.C.J. (2010). An efficient method of directly cloning chimpanzee adenovirus as a vaccine vector. Nat. Protoc. *5*, 1775–1785. https://doi.org/10.1038/nprot.2010.134.

STAR★METHODS

KEY RESOURCES TABLE

REAGENT or RESOURCE	SOURCE	IDENTIFIER
Antibodies		
Rabbit polyclonal anti-PEDF	Sino Biological	Cat#11104-RP02
Rabbit polyclonal antibody anti-VEGFR1	Affinity	Cat#AF7748
Rabbit polyclonal anti-CD59	Sino Biological	Cat#12474-RP02
Rabbit polyclonal anti-p44/42 MAPK (Erk1/2)	Cell Signaling Technology	Cat#9102
Mouse monoclonal anti- Phospho-p44/42 MAPK (Erk1/2) (Thr202/Tyr204) (E10)	Cell Signaling Technology	Cat#9106
Rabbit monoclonal anti-p38 MAPK (D13E1)	Cell Signaling Technology	Cat#8690
Rabbit monoclonal anti-Phospho-p38 MAPK (Thr180/Tyr182) (12F8)	Cell Signaling Technology	Cat#4631
Rabbit polyclonal anti-ICAM-1	Proteintech	Cat#10831-1-AP
Mouse monoclonal anti-VCAM-1	Santa Cruz biotechnology	Cat#sc-13160
Mouse monoclonal anti-GAPDH	Proteintech	Cat#HRP-60004
Hamster monoclonal anti-CD31	Millipore	Cat#MAB1398Z
Rabbit monoclonal anti-F4/80	Cell Signaling Technology	Cat#30325S
Mouse monoclonal anti-C5b-9	Santa Cruz Biotechnology	Cat#sc-66190
Rat monoclonal anti-BrdU	Abcam	Cat# ab6326
Goat polyclonal anti-mouse H&L (HRP)	Abcam	Cat#ab6789
Goat polyclonal anti-rabbit H&L (HRP)	Abcam	Cat#ab6721
Goat polyclonal anti-armenian hamster, Alexa Fluor 594	Jackson ImmunoResearch	Cat#127-585-099
Donkey polyclonal anti-rabbit, Alexa Fluor 488	Jackson ImmunoResearch	Cat#711-545-152
Donkey polyclonal anti-mouse, Alexa Fluor 488	Jackson ImmunoResearch	Cat#715-545-150
Donkey polyclonal anti-rat, Alexa Fluor 594	Jackson ImmunoResearch	Cat#712-585-150
Bacterial and virus strains		
AdC68-empty	This paper	N/A
E.coli Stbl2 Chemically Competent Cell (JM109 strain)	Shanghai Weidi Biotechnology Co., Ltd	Cat#DL1045
Chemicals, peptides, and recombinant proteins		
SrfI	New England Biolabs	Cat#R0629S
PI-SceI	New England Biolabs	Cat#R0696S
I-CeuI	New England Biolabs	Cat#R0699S
PacI	New England Biolabs	Cat#R0547L
ApaI	New England Biolabs	Cat#R0114S
MfeI-HF	New England Biolabs	Cat#R3589L
XhoI	New England Biolabs	Cat#R0146S
2×RealStar Power SYBR qPCR Mix (UNG)	Genstar	Cat#A312
X-tremeGENE™ HP DNA Transfection Reagent	Roche	Cat#6366236001
5-Bromo-2-deoxyuridine (BrdU)	Sigma-Aldrich	Cat#B5002
VEGF	R&D	Cat#293-VE
LPS	Sigma-Aldrich	Cat#L2630
protease inhibitor cocktail	APExBIO	Cat#K1007
phosphatase inhibitor cocktail	APExBIO	Cat#K1015

(*Continued on next page*)

Continued

REAGENT or RESOURCE	SOURCE	IDENTIFIER
Critical commercial assays		
EndoFree Mini Plasmid Kit II	TIANGEN	Cat#DP118-02
Gel Extraction Kit	Omega	Cat#D2500-02
GenRec Assembly Master Mix Kit	General Bio	Cat#CL08050
TIANamp Genomic DNA Kit	TIANGEN	Cat#DP304-03
Experimental models: Cell lines		
293A	ATCC	Cat#CRL-1573
ARPE-19	ATCC	Cat#CRL-2302
HUVEC	This paper	N/A
Experimental models: Organisms/strains		
Vldlr$^{-/-}$ mice	This paper	N/A
Oligonucleotides		
qPCR Primer: Human PEDF Forward: 5'-CAAGGTGCCCGTGAACAAAC-3'	This paper	N/A
qPCR Primer: Human PEDF Reverse: 5'-CTCCTTGTAGGTCCCGTGGAT-3'	This paper	N/A
qPCR Primer: Human sFlt-1 Forward: 5'-CATCATCAGCAACGCCACCTAC-3'	This paper	N/A
qPCR Primer: Human sFlt-1 Reverse: 5'- TTCTTCTTCTCACGCTGGCTCT-3'	This paper	N/A
qPCR Primer: Human sCD59 Forward: 5'-GATTTCGACGCCTGCCTGAT-3'	This paper	N/A
qPCR Primer: Human sCD59 Reverse: 5'-CAGTCTGGTGGTCACGTCGTTG-3'	This paper	N/A
Recombinant DNA		
AdC68-PEDF-P2A-sFlt-1-P2A-sCD59 (AdC68-PFC)	This paper	N/A
AdC68-eGFP	This paper	N/A
Software and algorithms		
GraphPad Prism 9.0	GraphPad Software	https://www.graphpad.com/
SnapgGene 7.0	GSL Biotech	https://www.snapgene.com/
ImageJ	National Institutes of Health	https://imagej.nih.gov/

RESOURCE AVAILABILITY

Lead contact

Further information and requests for resources and reagents should be directed to and will be fulfilled by the Lead Contact Prof. Hua Yan (zyyyanhua@tmu.edu.cn).

Materials availability

Plasmids, viruses and animal models generated in this paper will be shared freely upon request to the lead contact.

Data and code availability

Data: All data reported in this paper will be shared by the lead contact upon request.
Code: This paper does not report original code.
Any additional information reported in this paper is available from the lead contact upon request.

EXPERIMENTAL MODEL AND STUDY PARTICIPANT DETAILS

Animals

All study protocols involving animal use were approved by the Institutional Animal Care and Use Committee of Tianjin Medical University (approval number: TMUaMEC 2022006). All the mice were treated in accordance with the Association for Research in Vision and Ophthalmology (ARVO) Statement for the Use of Animals in Ophthalmic and Vision Research. Male C57BL/6J mice of 6–8 weeks old were purchased from the Vital River Laboratory Animal Technology Co., Ltd. (Beijing, China). *Vldlr*$^{-/-}$ mice were generated according to the structure of the Vldlr gene, and exon2-exon11 of Vldlr-207 (ENSMUST00000167487.7) transcript was knocked out using CRISPR/Cas9 technology. All mice were housed in specific pathogen-free (SPF) animal facilities, which have standardized conditions with a 12-h light/12-h dark cycle, at Tianjin Medical University, Tianjin, China.

Laser-induced CNV model

After anaesthesia and pupil dilatation, four laser burns were induced using an Nd: YAG laser (LB-002088 REV B, Lumenis, USA) around the optic disk at the 3, 6, 9, and 12 o'clock positions. The laser settings were as follows: 100 μm spot size, 0.15 s exposure time, and 200 mW power. The generation of a bubble demonstrated the rupture of Bruch's membrane, which confirmed the successful laser burn. To analyse CNV and macrophage infiltration areas, RPE-choroid flat mounts stained with CD31 and F4/80 were performed on days 7 and 14 after laser burn.

Cell cultures

HEK293A cells were purchased from the American Type Culture Collection (ATCC). ARPE-19 cells were obtained from Qianzhikang Laboratory (Public Health Clinical Center, Shanghai, China). HUVECs were cultured in ECGM (QiDa Biotechnology, Shanghai, China) supplemented with 5% FBS, 1% cell growth factor and 1% Gentamicin/Amphotericin, and were used from passages 2–6.[63] HEK293A and ARPE-19 cells were maintained in complete Dulbecco's modified Eagle's medium (DMEM; HyClone, Logan, UT, USA) supplemented with 10% (v/v) foetal bovine serum (FBS; EallBio, China), 100 U/mL penicillin, and 100 μg/mL streptomycin. All cells were incubated at 37°C under 5% CO_2. For the stimulation experiments, HUVECs were cultured in starved ECGM supplemented with 1% FBS.

To study the role of AdC68-PFC in MAPK pathway activation, 2×10^5 HUVECs were pre-treated with PBS (negative control), 1×10^{10} vp AdC68-empty, and 1×10^{10} vp AdC68-PFC for 48 h in starvation medium at 37°C. In the conbercept (positive control; KANGHONG, China)-treated wells, cells were pre-treated with 10 μg conbercept for 5 min before VEGF stimulation. HUVECs were then stimulated with VEGF (50 ng/mL; R&D Systems, US) for 10 min. To test the effect of AdC68-PFC on endothelial inflammation, 2×10^5 HUVECs were pre-treated with PBS (negative control), 1×10^{10} vp AdC68-empty, or 1×10^{10} vp AdC68-PFC for 40 h in starvation medium and then stimulated with LPS (1 μg/mL, Sigma, US) for 8 h. In the conbercept (positive control)-treated wells, HUVECs were pre-treated with 10 μg conbercept for 5 min after LPS stimulation.

METHOD DETAILS

Vector production

Recombinant adenoviral AdC68 vectors were generated via one-step isothermal assembly, as previously described.[64] AdC68 vectors incorporating eGFP and AdC68 vectors incorporating PEDF, sFlt-1, and sCD59 were constructed, and the cleavable linker P2A was used for the connection of two different genes. In brief, human PEDF, sFlt-1, sCD59, and P2A sequences were codon-optimized and synthesized by TSINGKE (Beijing, China) and inserted into the E1-deleted region of the replication-deficient adenoviral vector AdC68, driven by a modified human cytomegalovirus major immediate early promoter (IE CMV). Finally, AdC68-PEDF-P2A-sFlt-1-P2A-sCD59 (AdC68-PFC) was generated. The eGFP gene was also inserted into the E1-deleted region of AdC68, driven by the IE CMV promoter, to generate AdC68-eGFP. AdC68-empty was used as a sham control, with no insertion at the E1-deleted locus. Recombinant adenoviruses were rescued and amplified in HEK293A cells and purified by CsCl gradient ultracentrifugation. Viral particles were calculated by measuring UV absorbance at 260 nm (A260) using spectrophotometry: vp = $OD_{260}\times$dilution$\times1.1\times10^{12}$. Adenoviral vectors were confirmed by restriction enzyme digestion and DNA fragments were sequenced to ensure correct ligation.[65]

PEDF, sFlt-1, and sCD59 expression analyses

To analyse the *in vitro* expression of PEDF, sFlt-1, sCD59, ARPE-19 cells, and HUVECs were cultured and seeded in 6-well plates and then infected with AdC68-PFC at varying doses of 1×10^8 vp, 1×10^9 vp, and 1×10^{10} vp each well, and 1×10^{10} vp of AdC68-empty was used as the control group. Cells and supernatants were harvested for western blotting 48h post-infection and stored at -80°C for protein extraction and subsequent immunoblotting.

To analyse the *in vivo* expression of PEDF, sFlt-1, and sCD59, each mouse was injected in the right eye of 7.5×10^9 vp AdC68-PFC, and the left eye without injection was used as the control group. Seven days after the IVT injection, the retina-choroid-sclera complexes were dissected and lysed in ice-cold lysis buffer (RIPA; R0010; Solarbio, China) for subsequent immunoblotting.

IVT injection

For the preventive strategy, laser induction was performed 4 days after PBS and AdCs injection, and 1 d after the conbercept injection. As a therapeutic strategy, laser induction was performed 1 d before IVT injection. The IVT injections were performed using a 33-gauge syringe needle (Hamilton, US). For the preventive strategy, 1.5 μL PBS or buffer containing 1.5×10^9 vp AdCs was delivered by each calibrated micropipette 4 days before the laser, and 1.5 μL conbercept (10 mg/mL) was delivered 1 d before the laser. For the therapeutic strategy, 1.5 μL PBS, 1.5 μL buffer containing 1.5×10^9 vp/7.5×10^9 vp AdCs, or 1.5 μL conbercept (10 mg/mL) were delivered by each calibrated micropipette 1 day after laser. For adult (6–8 week) *Vldlr*$^{-/-}$ mice, 1.5 μL PBS, 1.5 μL buffer containing 1.5×10^9 vp AdCs, and 1.5 μL conbercept (10 mg/mL) were injected intravitreally. For P10 *Vldlr*$^{-/-}$ mice, 0.8 μL PBS, 0.8 μL buffer containing 0.8×10^9 vp AdCs, and 0.8 μL conbercept (10 mg/mL) were injected intravitreally.

In vivo fluorescence imaging

Male C57BL/6J mice of 6–8 weeks old were observed weekly for five weeks after AdC68-eGFP administration. eGFP expression in the mouse eye was observed using a Micron IV Retinal Imaging Microscope (Phoenix Research Labs, Pleasanton, CA, USA).

FFA

For laser-induced CNV model mice, FFA was performed using Heidelberg confocal retinal angiography (Heidelberg, Spectralis HRA, Germany) at 7 and 14 days after laser irradiation. After pupil dilatation with compound tropicamide eye drops, the mice were anaesthetized and 0.1 mL/kg 10% fluorescein sodium (Alcon Research LLC, US) was injected intraperitoneally. FFA images were acquired 2 min after the injection of fluorescein sodium.

For adult *Vldlr*$^{-/-}$ mice, FFA was performed 7, 14, and 35 days after IVT injection using a Micron IV Retinal Imaging Microscope (Phoenix Research Laboratories, Pleasanton, CA, USA). Similarly, the pupils were dilated, the mice were anaesthetized, and fluorescein sodium (Alcon Research LLC, US) was injected intraperitoneally. FFA images were acquired 2 min after the injection of fluorescein sodium. All FFA images were analysed using FIJI/Image J (NIH, US) software.

Immunofluorescence

Mouse eyeballs were fixed in 4% paraformaldehyde (PFA) for 45 min at room temperature (RT). Then, the RPE-choroid complexes were dissected, permeabilized 1% TritonX-100 overnight at 4°C then blocked with 2% BSA, 0.3% TritonX-100 in PBS for 12 h at 4°C. Subsequently, the tissues were incubated with proper primary antibodies for two days at 4°C: hamster anti-CD31 monoclonal antibody (1:150, MAB1398Z, Millipore, US), rabbit anti-F4/80 monoclonal antibody (1:200, 30325S, Cell Signaling Technology, US), and mouse anti-C5b-9 monoclonal antibody (1:100, sc-66190, Santa Cruz Biotechnology, US). After three washes in PBS, the tissues were incubated with the corresponding secondary antibodies (1:300, Jackson ImmunoResearch, US) for 2 h at RT. After washing with PBS overnight at 4°C, the RPE-choroid complexes were flat-mounted with mounting medium on glass slides.

For flat-mounted retinas, the eyes of the mice were enucleated and fixed in 4% PFA for 1 h at RT, and then the retinas were dissected. After washing with PBS, the retinas were permeabilized with PBS containing 1% TritonX-100 overnight at 4°C then blocked in PBS containing 5% BSA, 0.5% TritonX-100 for 12 h at 4°C. The flat-mounted retinas were stained with isolectinGS-IB4 (1:100) for 3 h at RT. After washing with PBS containing 0.1% TritonX-100 overnight at 4°C, the retinas were flat-mounted with mounting medium on glass slides.

The immunostaining of choroidal and retinal flat mounts was captured using a confocal fluorescence microscope (LSM 900, Carl Zeiss, Germany) and analysed using the FIJI/ImageJ software.

Western blot assay

Tissues and cells were lysed in 200 μL RIPA buffer containing protease inhibitors (Roche) and the supernatant was filtered (0–20 mm). Then, equal protein was loaded and electrophoresed in 8–15% SDS-polyacrylamide gel electrophoresis (SDS-PAGE) and transferred to a PVDF membrane (IPVH00010, Millipore, USA). PVDF membranes were blocked with 5% milk in PBST (PBS+Tween-20) for 2 h at RT and then target proteins were detected by specific primary antibodies including PEDF (1:500, 11104-RP02, Sino Biological, China), VEGFR1 (1:500, AF7748, Affinity, US), sCD59 (1:500, 12474-RP02, Sino Biological, China), Erk1/2 p44/42 (1:1000, 9102, Cell Signaling Technology, US), Erk1/2 phospho-p44/42 (T202/Y204) (1:1000, 9106, Cell Signaling Technology, US), p38 MAPK(1:1000, 8690, Cell Signaling Technology, US), Phospho-p38 MAPK (Thr180/Tyr182) (1:1000, 4631, Cell Signaling Technology, US), ICAM-1 (1:1000, 10831-1-AP, Proteintech, US), VCAM-1 (1:200, sc-13160, Santa Cruz biotechnology, US). HRP-Conjugated GAPDH Monoclonal Antibody (1:10000, HRP-60004, Proteintech, US) was used as an internal control. FIJI/Image J software was used to quantify the WB bands. The protein expression values were normalized to that of GAPDH. Each experiment was performed at least thrice.

RNA extraction, complementary DNA synthesis, and quantitative real-time qPCR analysis

The eyes of mice were enucleated 4 days after administration of 1.5×10^9 vp or 7.5×10^9 vp AdC68-PFC. Each mouse was injected into the right eye; the left eye with no injection was used as the control group. Retina-choroid complexes were dissected and homogenized in TRIzol® reagent (Invitrogen, US). RNA samples were reverse-transcribed to complementary DNA (cDNA) using the StarScript II RT Mix with gDNA Remover (GenStar, China). qPCR was performed using 2×RealStar Power SYBR qPCR Mix (GenStar, China) and processed with the

QuantStudio 5 Real-Time PCR system (Applied Biosystems, US). The primers used in this study were as follows: human PEDF forward, 5'-CAAGGTGCCCGTGAACAAAC-3'; human PEDF reverse, 5'-CTCCTTGTAGGTCCCGTGGAT-3'; human sFlt-1 forward, 5'-CATCATCAG CAACGCCACCTAC-3'; human sFlt-1 reverse, 5'- TTCTTCTTCTCACGCTGGCTCT-3'; human sCD59 forward, 5'-GATTTCGACGCCTGCCT GAT-3'; and human sCD59 reverse, 5'-CAGTCTGGTGGTCACGTCGTTG-3'. The absolute number of mRNA copies was calculated using a standard curve method.

The BrdU incorporation assay in ECs

To analyze EC proliferation *in vitro*, the BrdU incorporation assay was performed. Briefly, HUVECs were cultured on collagen-coated coverslips in 24-well plates and pre-treated with PBS, 2.5×10^9 vp AdC68-empty, or 2.5×10^9 vp AdC68-PFC for 24 h in starvation medium. Cells were then treated with or without VEGF (50 ng/mL) for 24 h. BrdU (10 μM, B5002, Sigma-Aldrich, US) was added 4 h before PFA fixation. The cells were then permeabilized and blocked in PBS containing 2% BSA and 0.3% TritonX-100 for 30 min at RT. Unmasking was performed by adding ice-cold 0.1 M HCl for 20 min followed by 2 M HCl for 30 min. Neutralization was performed with sodium borate buffer (0.1 M Na2B4O7 in water, PH8.5) for 15 min, prior to primary antibody incubation. An anti-BrdU antibody (1:250, ab6326, Abcam, UK) was incubated in blocking solution overnight at 4°C, and appropriate secondary antibody (1:400, Alexa Fluor 594-conjugated, Jackson ImmunoResearch, US) was incubated for 2 h at RT. Nuclei were counterstained with DAPI (1:1000, D1306, Invitrogen). Images were obtained using a fluorescence microscope (CKX53; Olympus). Quantification was performed blinded to the experimental conditions. Four biological replicates were used for quantification.

Scratch assay

To analyse EC migration, HUVECs were cultured in collagen coated in 6-well plates. When cells were confluent, they were infected with 1×10^{10} vp AdC68-empty or 1×10^{10} vp AdC68-PFC for 48 h in starvation medium. A wound was made by scraping the cell monolayer with a 200 μL pipette tip, and the cells were stimulated with or without VEGF (50 ng/mL). Pictures were acquired at time-point zero and 12 h after incubation at 37°C. The percentage of wound closure between 0 and 12 h was analysed using FIJI/Image J software with investigators blinded to the experimental conditions. Eight biological replicates were used.

OCT

OCT was performed 35 days after IVT injection in 6–8-week-old male C57BL/6J mice using a Micron IV Retinal Imaging Microscope (Phoenix Research Labs, Pleasanton, CA, USA). The thickness of the retina around the optic disc was measured and calculated using built-in software.

TUNEL assay

TUNEL assay was used to examine apoptotic cells in retinas/choroids. Mice were sacrificed 35 days after the IVT injection, and the eyes from each group were enucleated. Eyes were fixed in 4% PFA for 2 h at RT. Afterwards, they were transferred to 30% sucrose/PBS at 4°C overnight and subsequently to OCT (Sakura, Japan) and frozen at -80°C. Serial 10 μm-thick sections were cut using a cryostat (CM1950, Leica, Germany). TUNEL assay was performed using a One Step TUNEL Apoptosis Assay Kit (C1088, Beyotime, China) according to the manufacturer's instructions.

QUANTIFICATION AND STATISTICAL ANALYSIS

All results are presented as mean ± SEM, and statistical analyses were performed using GraphPad Prism 8.0.1 (GraphPad Software). Comparison of data between groups was performed using Student's t-test (two-tailed) (when comparing two groups) or one-way ANOVA followed by Tukey's multiple comparisons test (when comparing three or more groups). Statistical significance was set at $P < 0.05$.